

Fabrication of Multizonal Scaffolds for Osteochondral Tissue Repair

A thesis presented to
the faculty of
the Russ College of Engineering and Technology of Ohio University

In partial fulfillment
of the requirements for the degree
Master of Science

Brett M. Hannon

May 2023

© 2023 Brett M. Hannon. All Rights Reserved.

This thesis titled
Fabrication of Multizonal Scaffolds for Osteochondral Tissue Repair

by

BRETT M. HANNON

has been approved for
the Department of Chemical and Biomolecular Engineering
and the Russ College of Engineering and Technology by

Mei Wei

Professor of Mechanical Engineering

Maj Mirmirani

Interim Dean, Russ College of Engineering and Technology

Abstract

HANNON, BRETT M., M.S., April 2023, Biomedical Engineering

Fabrication of Multizonal Scaffolds for Osteochondral Tissue Repair

Director of Thesis: Mei Wei

A study on a solution to repair osteochondral defects was investigated. This work contained the use of a novel collagen-based biomaterial that was structured to mimic the composition and structure of osteochondral tissue. Collagen extraction from the bovine achilles was optimized in terms of atelocollagen yield and stability. It was found that collagen enzymatically digested at a 1.25:10 pepsin to tendon weight ratio in the superior tendon region, gave optimal results in terms of atelocollagen quantity and hydrogel formation. Mineralized collagen scaffolds were fabricated to reflect the composition of subchondral bone. Controlled freezing was applied, which successfully oriented collagen fibers mimicking those in each native zonal tissue. Multiple approaches were attempted to replicate the collagen orientations of osteochondral tissue, ultimately a T-shaped mold was designed to guide directional freezing, resulting in an anisotropic scaffold structure. Native composition of bone hydroxyapatite and cartilage hyaluronic acid were also taken into consideration when fabricating such multizonal scaffolds.

Dedication

I would like to thank my mother, Angela, and my father, Matthew, for their constant support and love. I am grateful of the values of perseverance and persistence that you have instilled upon me. I'd also like to thank my brother, Ben, and sister, Ally, each of you have such bright futures ahead and I am so proud to call you, my siblings. I'd like to thank my grandparents, Marlinda and William, for your constant affection towards my siblings and me.

Acknowledgments

I would like to start by thanking my major advisor, Dr. Mei Wei. Her guidance to helping me grow not only academically and professionally but also opening my horizons to many future opportunities. Her advice and motivation have pushed me to be better myself as an individual.

I would also like to thank my committee members, Dr. Doug Goetz, Dr. Andrew Weems, and Dr. Shouan Zhu. Each of them have been available when needed and helped me present information in an efficient manner.

I would also like to thank each of my lab mates Dr. Le (Jasper) Yu and Dr. Sacha Cavelier. Jasper, your knowledge and experience of biomaterials have helped me tremendously. Sacha, your expertise in collagen and bone biology have supported me to my position today.

Also, I would like to thank those who have helped train or lended equipment to make this project possible: Dr. Damilola Daramola and Dr. Maryam Eslami for use of SEM and EDS, Mr. Mohiedin Bagheri Hariri for the assistance of XRD, Mr. Javad Shokraiyan for help of FTIR, Dr. Kody Wolfe for assistance of TGA, and lastly but not least, Mr. Thomas Boyle and Ms. Kate Willhelm for the fabrication of the PMMA molds.

Table of Contents

	Page
Abstract.....	3
Dedication.....	4
Acknowledgments.....	5
List of Tables	8
List of Figures	9
Chapter 1 - Background.....	11
1.1. The Material Cartilage	11
1.1.1. Cartilage Composition and Structure	11
1.1.2. Current Practice for Cartilage Repair and Regeneration.....	13
1.2. Collagen	18
1.2.1. Collagen Type I Structure and Properties	18
1.2.2. Use of Collagen Type I for Biomedical Applications.....	20
1.3. Multizonal Scaffolds Fabrication.....	22
1.3.1. State-of-the-Art of Multizonal Scaffolds	22
1.4. Objectives of the Thesis.....	24
1.4.1. Hypothesis.....	24
1.4.2. Short-Term Goals.....	24
Chapter 2 - Extraction of Bovine Achilles Collagen Type I.....	26
2.1. Introduction.....	26
2.1.1. Pepsin Digestion.....	27
2.1.2. Bovine Collagen and Its Applications.....	29
2.2. Methods and Materials.....	31
2.2.1. Pepsin Digestion of Bovine Type I Collagen.....	32
2.2.2. Pepsin Deactivation and Salt Bath	33
2.2.3. Redissolution and Dialysis	34
2.3. Results.....	35
2.4. Discussion.....	39
2.5. Conclusion	46
Chapter 3 - Fabrication of Collagen Hydroxyapatite Lamellar Scaffold.....	47
3.1. Introduction.....	47

3.1.1. Biocompatibility.....	47
3.1.2. Porosity & Pore Size.....	48
3.2. Methods and Materials.....	49
3.2.1. Gelation, Self-Compression, and Freeze Drying.....	49
3.2.2. Scaffold Crosslinking.....	50
3.2.3. Scaffold Characterization.....	51
3.3. Results.....	52
3.3.1. Characterization of Mineralized Collagen Lamellar Scaffolds.....	55
3.4. Discussion.....	59
3.5. Conclusion.....	62
Chapter 4 - Fabrication of Multizonal Scaffold.....	63
4.1. Introduction.....	63
4.1.1. Fabrication.....	64
4.2. Methods and Materials.....	67
4.2.1. Scaffold Characterization.....	71
4.3. Results.....	71
4.3.1. Characterization results.....	72
4.4. Discussion.....	76
4.5. Conclusions.....	79
Chapter 5 - Summary/Future Directions.....	80
Chapter 6 - References.....	81

List of Tables

	Page
Table 1.1. Examples of collagen applications in the biomedical field (Rezvani Ghomi et al., 2021)	20
Table 2.1. Extraction protocols	33
Table 2.2. Effect of pepsin and acetic acid concentrations on collagen yield	36
Table 2.3. Bovine tendon yields and their gelation capabilities.	38
Table 3.1. Scaffold attempts based on pepsin/tendon ratios of superior region collagen. 54	54
Table 3.2. Scaffold attempts based on pepsin/tendon ratios of inferior region collagen.. 54	54
Table 3.3. Scaffold attempts based on pepsin/tendon ratios of mixed region collagen.... 55	55
Table 4.1. Multizonal scaffold fabrication methods and their respective compositions. . 70	70
Table 4.2. Visual results of each multizonal method. (a) HyA suspension + dried HA scaffold. (b) HyA suspension + HA gel. (c) HyA scaffold + HA scaffold bonded by BioGlue.	72

List of Figures

	Page
Figure 1.1. Articular cartilage layers with collagen fibers and chondrocytes organization and orientation (Killen & Charalambous, 2020).....	13
Figure 1.2. (a) Structure of collagen molecule to a tendon fiber. (b) Collagen fascicle structure. (c) Collagen fibril structure. (d) Collagen molecule structure (Fratzl, 2003)...	19
Figure 2.1. Pepsin activity based on pH (Piper & Fenton, 1965).	28
Figure 2.2. Bovine achilles tendon separation.	30
Figure 2.3. Extraction of bovine collagen. (a) Mechanical separation of bovine tendons. (b) Pepsin treatment. (c) Pepsin deactivation and salt bath. (d) Redissolution of collagen and dialysis.....	32
Figure 2.4. Pepsin treated collagen solution after initial centrifugation.	34
Figure 2.5. Pepsin/tendon ratio (g/g) and tendon/acetic acid ratio (g/mL) yield.	36
Figure 2.6. (a) Type I collagen molecular structure, (b) Atelocollagen formation through pepsin digestion, (c) Gelation of atelocollagen, (d) Fibrillogenesis formation of collagen, (e) Denaturation of collagen, and (f) Hydrolysis to collagen peptides (Cavelier et al., 2023).	43
Figure 2.7. Achilles tendon anatomy.	44
Figure 3.1. Fabrication of collagen-hydroxyapatite lamellar scaffold. (a) Collagen-mineral solution preparation. (b) 37°C water bath and gelation of the suspension. (c) Self-compression. (d) Radial freezing and freeze-drying	51
Figure 3.2. Collagen hydroxyapatite lamellar scaffold. (a) Scaffold before crosslinking process. (b) Scaffold after crosslinking process. (c) Thickness of scaffold after crosslinking. (d) Lamellar structure of scaffold.....	53
Figure 3.3. SEM images of a lamellar scaffold imaged at two different scales: (a) x40 and (b) x75.....	55
Figure 3.4. Elemental analysis of collagen hydroxyapatite lamellar scaffold.	56
Figure 3.5. FTIR spectra of collagen hydroxyapatite lamellar scaffold with specific peaks.	57
Figure 3.6. XRD of a mineralized collagen lamellar scaffold.	58
Figure 3.7. TGA of collagen hydroxyapatite lamellar scaffold.	59
Figure 3.8. (a) Radial freezing of hydrogel. (b) Dendritic ice growth during directional freezing forces collagen fibers to arrange along a preferred direction. (c) Resulting scaffolds exhibit a lamellar structure mimicking the collagen arrangements in superficial and deep zones of cartilage tissue.....	60

Figure 4.1. Illustration of directional freezing of scaffolds zones. Following with lyophilization to mimic the zones of osteochondral tissue: Superficial zone (SZ), transition zone (TZ), calcified cartilage zone (CCZ), and osseous zone (OZ) (Clearfield et al., 2018).	64
Figure 4.2. (a) Comparison of compressive stress vs strain between varying directions of pores. (b) Comparison of compressive moduli between varying directions of pores. (Arora et al., 2015).....	66
Figure 4.3. T-shaped PMMA mold used for directional freezing.....	68
Figure 4.4. Combined SEM image of osseous zone (bottom) to superficial zone (top) of multizonal scaffold at x60 magnification.	74
Figure 4.5. FTIR of collagen-hydroxyapatite lamellar zone and collagen-hyaluronic acid zone of a multizonal scaffold.....	75
Figure 4.6. (a) Unidirectional freezing resulting in the superficial zone. (b) Homogenous freezing resulting in transition zone of a cellular structure.....	77
Figure 4.7. SEM image of collagen HyA scaffold and collagen HA scaffold with separation between layers for the second approach.....	78
Figure 4.8. SEM image of BioGlue used to integrate each scaffold. The circle area is the BioGlue, which has demonstrates a dense structure.....	79

Chapter 1 - Background

1.1. The Material Cartilage

1.1.1. *Cartilage Composition and Structure*

¹Cartilage, a support mechanism of the musculoskeletal system, is a flexible connective tissue that provides support and durability. Hyaline cartilage is the most common type of cartilage found in the human body (Poole et al., 2001). It contains primarily Type II collagen and is characterized by its lack of lymphatic vessels and avascularity giving a semitransparent appearance at its fresh state (Mescher, 2013; Poole et al., 2001). Articular cartilage is composed of hyaline cartilage which is located at the surfaces of joints and is surrounded superficially by a lubricant to reduce friction between adjacent bones. Its functions include transmitting mechanical loads at the joint location and aiding in bone movement (Wei & Dai, 2021). Articular cartilage only contains a total cell volume of approximately 2%. The remainder is occupied by the extracellular matrix (ECM) which is synthesized by chondrocytes (Poole et al., 2001). The ECM consists of water (68-85% of wet weight), collagen (60-85% of dry weight), proteoglycan (15-40% of dry weight), and some other minor proteins (Bhosale & Richardson, 2008; Chen et al., 2006; Huber et al., 2000).

Articular cartilage is composed of four separate layers which consist of: superficial, transition (middle), deep, and calcified cartilage layer as shown in Figure 1. Starting with the outermost layer, the superficial zone, it is in contact with the synovial fluid of the

¹ Portions of this work appeared in Yu, L., Cavelier, S., Hannon, B., & Wei, M. (2023). Recent development in multizonal scaffolds for osteochondral regeneration. *Bioact Mater*, 25, 122-159. <https://doi.org/10.1016/j.bioactmat.2023.01.012>

articular joints. The layer is divided into the lamina splendens and a cellular layer. The lamina splendens are part of the friction free surface and allow for joint mobility (Baumann et al., 2019). The cellular layer contains the highest amount of water and chondrocytes, and the collagen fibers are highly organized. The superficial zone consists of approximately 10-20% of the overall thickness of the cartilage (Sophia Fox et al., 2009). Deeper to the superficial zone, the largest zone of cartilage, is the middle layer. This layer differs from the superficial zone by having much thicker and organized obliquely collagen fibers (Sophia Fox et al., 2009). The main function of the layer is to support in resisting compressive forces applied on the articulating surfaces (Temenoff & Mikos, 2000). The middle zone consists of approximately 50% of the depth in cartilage (Baumann et al., 2019). Beneath the transitional zone is the deep zone. This zone is composed of collagen fibers that are the largest in diameter and are perpendicular to the cartilage surface. The organization of collagen is designed to resist against compressive forces applied to the joint (Sophia Fox et al., 2009). The deep zone consists of approximately 30% of the depth in cartilage and has the lowest amount of water between the zones at an estimated 65% (Baumann et al., 2019). Below the deep zone is the calcified cartilage layer, which is just above subchondral bone. Calcified cartilage is approximately 20 to 250 microns thick (Baumann et al., 2019). This layer combines characteristics of articular cartilage and subchondral bone for the purpose of aiding in the reduction of stress concentrations between the two (Temenoff & Mikos, 2000). This layer also contains a tidemark, as shown in Figure 1.1, that is permeable to small nutritional solutes to perform the task of maintaining the microenvironment between the deep layer and the calcified cartilage layer

(Temenoff & Mikos, 2000). The calcified cartilage layer has a unique role of anchoring collagen fibrils from the deep zone to the subchondral bone (Sophia Fox et al., 2009).

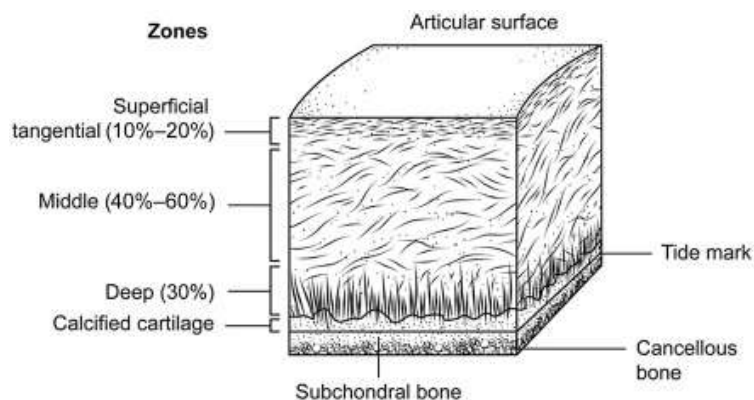


Figure 1.1. Articular cartilage layers with collagen fibers and chondrocytes organization and orientation (Killen & Charalambous, 2020).

1.1.2. Current Practice for Cartilage Repair and Regeneration

Articular cartilage lesions are one of the most encountered patient conditions in orthopedics. Once an osteochondral unit defect occurs, progression of the defect can lead to osteoarthritis (Baumann et al., 2019). Osteoarthritis can cause serious disability and pain to those it affects. It can be caused by genetic predisposition and/or can be induced by obesity, trauma, and normal wear and tear on the joints (Baumann et al., 2019). As osteoarthritis progresses, articular cartilage degenerates leading to painful bone-on-bone interactions. Cartilage injuries have been classified to the five main categories which include: normal chondral tissue (Grade 0), swelling of chondral tissue (Grade I), partial thickness chondral defects (Grade II), full thickness chondral defects (Grade III), and full thickness osteochondral defects (Grade IV) (Deng et al., 2019; Pereira et al., 2018; Temenoff & Mikos, 2000). In partial thickness defects, damage has been found at the

cartilage surface but does not extend to the subchondral bone. If such extension occurs, nearby cells proliferate, but it remains unclear the reasoning why cells attempt to fill the defect before it is repaired (Temenoff & Mikos, 2000). Full thickness chondral defects are involved with damage that extends across the entire cartilage thickness and stops at the subchondral bone plate (Pereira et al., 2018). In this injury, progenitor cells from bone marrow migrate to the damaged location to fill in the defect (Temenoff & Mikos, 2000). This causes the tissue to be less stiff and more prone to degradation over time. A full thickness osteochondral defect fissures through all cartilage and into subchondral bone. Treatment for each of these injuries varies by severity of defect and the individual patient's basis.

Cartilage repair and regeneration can be defined as restoring damaged tissue with new tissue as if it resembles the same composition, structure, and function (Seo et al., 2014). Some methods that have been studied including cell sourcing repair, cartilage restoration and regeneration, regeneration enhancement, and cartilage transplantation using autografts and allografts.

Cell sourcing repair is a process of using cells from a specific source to aid in osteochondral repair. The source must be easy to maintain and manipulate in vivo and have no limitations in accessibility. Some examples resources that are used are stem cells, such as mesenchymal stem cells (MSCs), and tissue-specific cells, such as chondrocytes or osteoblasts (Seo et al., 2014). Stem cells MSCs have been widely studied due to their high availability and capacity for differentiation and proliferation of osteochondral tissue repair. Tissue specific cells have also been a promising cell resource in osteochondral repair, but

without the use of osteochondral inductive factors, synthesis of each tissue has been difficult to attain (Seo et al., 2014).

Cartilage restoration and regeneration has been primarily attempted on patients with smaller lesions. The methods include replacement tissue grafts or assessing techniques that support native repair process in cartilage (Temenoff & Mikos, 2000). Cartilage regeneration is mainly used to combat the need of a donor site. This can be completed by enhancing the intrinsic regenerative properties of the tissue or transplantation of extra chondrocytes to aid in forming more tissue (Buckwalter & Mankin, 1998). Due to the complex structure of articular cartilage, restoration to its fully normal state is difficult to achieve (Baumann et al., 2019).

The most common treatment for cartilage repair and regeneration is regeneration enhancement (microfracture). This process involves penetrating the subchondral bone, thus creating a full thickness chondral defect. Once a clot forms over the bone surface, migration of native stem cells eventually transform into chondrocytes and osteocytes (Buckwalter & Mankin, 1998). Although outcomes of this treatment vary from creating fibrocartilage, hyaline cartilage, or even no cartilage, it has a small chance of harming the patient (Buckwalter & Mankin, 1998). A setback being, if hyaline cartilage is created, the mechanical properties and durability are less than the original tissue (Buckwalter & Mankin, 1998).

In cartilage transplantation of autografts, previous patients have had replaced localized regions of damaged cartilage surfaces with autografts vested from patella, femoral condyle, and proximal fibula (Temenoff & Mikos, 2000). The long-term results of

cartilage autografts have not been studied thoroughly, but generally there is limited availability for sites of harvest. This also restricts the treatments to smaller defects in cartilage and still raises concerns to the healing of the chondral portion of the auto graft to the adjacent cartilage (Temenoff & Mikos, 2000). Due to greater availability, osteochondral allografting is a more frequently used method. Studies have shown that fresh and frozen allografts can decrease joint pain (Gross et al., 2008). Additionally, the osseous section of the graft successfully heals to the host bone and the chondral section can perform normal to the articular cartilage surface (Temenoff & Mikos, 2000). A study on fresh osteochondral allograft specimens was conducted at Mount Sinai Hospital, University of Toronto. In the study, 126 fresh osteochondral allografts were used to treat posttraumatic osteoarticular defects in the knees of 123 patients. A 95% survival rate at 5 years, 80% at 10 years, and 65% at 15 years was reported (Gross et al., 2008). Another research on arthroscopic transfer of osteochondral allografts reported favorable results in frozen osteochondral allografts due to allowing time for testing of the donors for viral and bacterial infections (Buckwalter & Mankin, 1998). However, there are concerns with allogeneic and autogeneic implants that may compromise the patients immunology (Buckwalter & Mankin, 1998). Overall, cartilage transplantation of allografts seems to provide effective treatment for defects and degenerative involved in articular cartilage.

The future of cartilage grafts can be seen on the side of synthetic implants: many commercialized products are currently available or progressing through clinical trials for articular cartilage repair. For instance, NeoCart® from Histogenics, is a type I collagen scaffold that completed phase III of its clinical trials. 29 of the patients showed significant

improvements from a 5-year follow-up. However, 80% of the patients developed subchondral bone lesions such as, edema, cysts, sclerosis, and hypertrophy. Along with 14% of the patients showed no improvement from an MRI. These issues are suggested to be related to the removal of the calcified cartilage layer before implantation (Jiang et al., 2020). A product that is sold in European countries, Turkey, Iran, and China is CaReS® by Arthro Kinetics Biotechnology GmbH. This product involved using collagen type I hydrogels as scaffolds. In addition, the scaffold uses primary autologous chondrocytes as seed cells. From a short form survey (SF-36), functional knee scores were improved significantly from the baseline. However, low implant cell density resulted from the use of primary chondrocytes, which could negatively influence the effect of the cartilage regeneration (Jiang et al., 2020).

The parameters for successful cartilage repair and regeneration include (i) Biocompatibility and osteoconductivity: surface quality that promotes adhesion, negative immune response from the host, and growth of cells. The material must not induce an inflammatory tissue reaction or toxicity. (ii) Three-dimensional structure must be reproducible at large scale for the market. Porosity should be at least 90% to promote regeneration of the extracellular matrix. (iii) Material net should be replaced by natural tissue after serving its function. The degeneration rate must be in control to regulate regeneration rate of the desired tissue (Wirth & Rudert, 1996). (iv) Mechanical properties that can be obtained by cartilage regeneration from scaffold. Unfortunately, the ideal cartilage graft that satisfies all these conditions does not exist currently.

1.2. Collagen

1.2.1. *Collagen Type I Structure and Properties*

In hyaline cartilage the predominant collagen found is type II (Miosge et al., 2004). The loss of collagen type II and aggrecan has been primarily responsible for osteoarthritis and other hyaline cartilage diseases (Miosge et al., 2004). In contrast, collagen type I has been found in all stages of osteoarthritis, but especially in later stages as the disease progresses (Miosge et al., 2004).

Collagen type I is the most abundantly existing collagen. 70% of collagen found in the body is type I collagen (Xu et al., 2021). It is the basic building block of the structure in extracellular matrices, which are packed with collagen fibrils and fibril bundles that can be up to several hundred micrometers in diameter (Christiansen et al., 2000). The most common places that it can be found are in skin, ligaments, bone, and tendons. Each of these components of the body vary by strength, stiffness, and toughness, thus demonstrating how versatile collagen type I is for different applications (Fratzl, 2008). The basic structure of collagen contains three polypeptide α -chains which each consist of 1000 or more amino acids (Friess, 1998). These polypeptide chains form into triple helical protein chains (Fratzl, 2003). In collagen type I, the collagen molecule contains two polyproline-II α -chains which are identical, while the third heterotrimeric α -chain is homologous and chemically distinct (Parry, 1988; Xu et al., 2021). The polyproline-II α -chains are terminated by a short non-triplet-containing sequence called telopeptides (Parry, 1988). These telopeptides contain residue of hydroxylysine which are involved in the stabilization of molecular covalent cross-links (Parry, 1988). Collagen architecture organizes in four

levels of hierarchy which include: tendon fiber, fascicles, fibrils, and molecules. Collagen molecules are approximately 1.3 nm in diameter and 300 nm in length, as shown in Figure 1.2.d. Collagen molecules are assembled into collagen fibrils which range from 50-500 nm in diameter as shown in Figures 1.2.a and 1.2.c. The collagen fibrils are joined by a matrix with proteoglycans (Fratzl, 2003), which promote their assembly into 50-300 μm wide fascicles shown in Figures 1.2.a and 1.2.b. The collagen fascicles then make up the structure of a tendon fiber as shown in Figure 1.2.a (Fratzl, 2003).

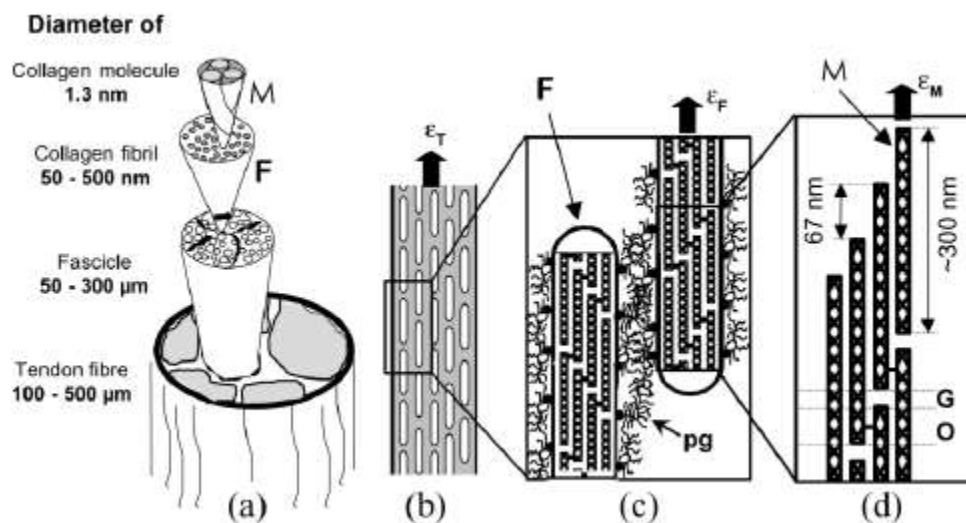


Figure 1.2. (a) Structure of collagen molecule to a tendon fiber. (b) Collagen fascicle structure. (c) Collagen fibril structure. (d) Collagen molecule structure (Fratzl, 2003).

A study, from the University of Medicine and Dentistry of New Jersey (Christiansen et al., 2000), was conducted by comparing collagen fibril diameters and their mechanical properties. The tests were performed for different pH, temperatures, and diameters. The results showed the most optimal mechanical properties were in acidic conditions ($\text{pH} < 7.0$) and temperatures lower than 30°C (Christiansen et al., 2000). Studies

have also demonstrated greater resistance to deformation of collagen fibrils at high strains, rather than low strains.

1.2.2. Use of Collagen Type I for Biomedical Applications

Collagen, a versatile substance in the medical field, can be used in many forms for many different applications as shown in Table 1.1.

Table 1.1. Examples of collagen applications in the biomedical field (Rezvani Ghomi et al., 2021)

Collagen as a Biomaterial	
Form	Applications
Gel	Cosmetic skin solutions
	Drug delivery
	Vitreous substitution
	Surgery
	Coats for prostheses
Sponge	3D cell culture
	Wound dressing
	Hemostatic agent
	Skin substitution
	Drug delivery
	Bone repair (rigid form)
Hollow fiber tubing	Cell culture
	Nerve regeneration
Sphere	Microcarrier for cell culture
	Drug delivery
Membrane	Drug delivery
	Dialysis
	Tissue regeneration
	Eye shield (cornea)
	Skin adhesives

Collagen based biomaterials can be used to enhance, maintain, or substitute biological tissues or organs to override the biological response of the damaged structures (Rezvani Ghomi et al., 2021). Collagen based scaffolds have become very popular in bone regeneration, cardiovascular repairs, and cartilage regeneration due to their biological and mechanical properties (Rezvani Ghomi et al., 2021). Some of the applications with collagen to be further discussed are tissue engineering, bone substitution, and drug delivery.

A variety of materials are used in biomedical applications such as metals, silicones, ceramics, polyglycolic acid (PGA), polylactic acid (PLA), copolymers, and natural polymers. Collagen based biomaterials separate from these materials by their biocompatibility (Muthukumar et al., 2018). Due to native collagen biological properties, it is provoked to function as a cell scaffold for tissue engineering application (Muthukumar et al., 2018). Fabrication of porous and dense collagen membranes have been carried out by processes of air-dry and freeze drying. Collagen and fibrin in hydrogel scaffolds have played an important role in promoting differentiation on adipose stem cells (Muthukumar et al., 2018).

In addition, collagen has been beneficial in the treatment of the cardiovascular system pathologies. Two main issues that arise in vascular disease are cardiovascular malfunction and venous/arterial pathologies. Tissue engineering solutions, in terms of heart diseases, rely on acellular matrix colonization and implantation of the heart (Parenteau-Bareil et al., 2010). An approach that has been developed at the LOEX group by Auger, involves using the patient's own cells to reconstruct living tissue-engineered blood vessels

(L'Heureux et al., 1998). The strategy consists in using human fibroblasts to create an extracellular matrix from their own collagen. The fibroblast sheet is then rolled into a tubular formation to produce a living vessel with ideal mechanical strength and biological properties. This tissue-engineered blood vessel has been successfully grafted on patients.

Another important application of collagen scaffolds is bone tissue engineering. The main composition of bone consists of collagen, calcium phosphate, water, and proteins. When a bone is dramatically damaged and cannot heal itself, one strategy is to replace the defect by a synthetic bone graft, such as a collagen based scaffold, to maintain its mechanical integrity (Rezvani Ghomi et al., 2021). Collagen based scaffolds are necessary when osteochondral defects reach a certain volume or when an autograft must be avoided due to pathological or practical reasons (Parenteau-Bareil et al., 2010). These bone grafts rely on the hardening of collagen as biomaterial by mineralization of calcium phosphate and crosslinking with other substances such as hydroxyapatite (Parenteau-Bareil et al., 2010). The collagen-based bone grafts are popular due to bone forming efficacy and promotion of cell growth.

1.3. Multizonal Scaffolds Fabrication

1.3.1. State-of-the-Art of Multizonal Scaffolds

Multizonal scaffolds have been a gold standard for treatment of osteochondral repair. This process involves several different layers which can mimic the subchondral bone, deep, transition, and superficial layers of articular cartilage. Each layer varies by lamellae orientation and composition of the extracellular matrix macromolecules throughout the tissue (Clearfield et al., 2018). Many groups are progressively working

towards a solution composing of polymers, metals, and collagen. Recently, the Tamaddon et al. 2021 group, fabricated a trilayered scaffold for osteochondral repair. The design involved a Ti6Al4V alloy matrix serving as the osseous zone, an ultrasonic welded PLA zone acting as the calcified cartilage component, and a polylactic-co-glycolic-acid (PLGA)-collagen casted section serving as the cartilage layer (Tamaddon et al., 2022). The Ti6Al4V alloy and PLA zones were 3-D printed via direct metal laser sintering and fueled deposition modeling. Another group from the Carl Gustav Carus Medicine and University created a multi-layered scaffold based on 3D bioplotting. Their design included a three layer scaffold that consisted of calcium phosphate cement (CPC) and alginate-methylcellulose (algMC). The superficial layer was primarily composed of algMC, the osseous layer primarily consisted of CPC that was seeded with osteogenic cells, and the calcified cartilage layer was fabricated as an interwoven network between each of the materials, algMC and CPC (Kilian et al., 2020).

1.3.1.1. Advantages

Besides the microstructural and mechanical properties of mineralized collagen scaffolds, a main advantage of multizonal structure, resides in its anisotropy. Many biomaterials for osteochondral repair are isotropic. When anisotropic matrices are implemented, this structure recapitulates the zonal layers of osteochondral tissue (Clearfield et al., 2018).

1.3.1.2. Current Limitations

Though there are many advantages to multizonal scaffolds, there are some limitations with this method of articular cartilage repair. Donor site morbidity and limited quantity of host tissue causes integration issues between the host and graft tissue (Levingstone et al., 2014). Proper chondrogenesis and mineralization of the cartilage and subchondral bone layers also is an issue between many modern solutions (Jia et al., 2018; Kilian et al., 2020). In addition, the degradation of the graft tissue arises as an issue (Levingstone et al., 2014). Commonly used metals, such as titanium alloy, for subchondral bone defects will not degrade long-term (Tamaddon et al., 2022). Which is not practical for all instances, especially small osteochondral defects. Previously reported mechanical properties are not comparable to natural cartilage in tension or flexion. In addition, many solutions do not properly mimic the native cartilage collagen orientation.

1.4. Objectives of the Thesis

1.4.1. Hypothesis

The main objective of this work is to create a bovine type I collagen-apatite composite, multizonal scaffold that mimics the structure and composition of each individual zone of the osteochondral tissue. We want to verify the hypothesis that a multizonal scaffold can meet the requirements.

1.4.2. Short-Term Goals

The short-term goals for this study would include:

- Identification and extraction of bovine type I collagen suitable for scaffold fabrication.
- Fabrication of mineralized scaffolds with the following properties:
 - Controlled porosity and lamellar architecture.

- Fabrication of multizonal collagen-based scaffolds that satisfy the following:
 - Mimics the anisotropic structure of each zone in the osteochondral tissue.
 - Mimics the composition of each zone in the osteochondral tissue.

Chapter 2 - Extraction of Bovine Achilles Collagen Type I

2.1. Introduction

Collagen type I can be extracted from several sources including; marine origin, bovine, rodents, avian, porcine, and humans (Rezvani Ghomi et al., 2021), and collagen is obtained via a chemical or enzymatic hydrolysis. In this study, bovine collagen type I is selected due to its abundance, and good structural and mechanical properties. The extraction and purification of bovine collagen type I involves the use of enzymes to break down non-collagenous proteins and other components of the tissue, followed by purification methods, such as precipitation and chromatography. Nevertheless, bovine collagen has significant composition variability in raw bovine tissue, so the extraction and purification of bovine collagen type I is a critical step determining its usefulness in forming tissue engineering scaffolds for biomedical applications. Bovine collagen has some advantages comparing to other sources, including large collagen fiber diameters, and high strains and high force at break (Zeugolis et al., 2008). It is believed that these high mechanical values are a result of the bovine achilles everyday function, withstanding high amounts of loading very frequently.

The extraction of bovine collagen type I typically begins with the acquisition of raw bovine tissue, such as skin or tendons (Aukkanit & Garnjanagoonchorn, 2010; Ju et al., 2020). Before the extraction a pretreatment must be performed using an acid or alkaline process to remove non-collagenous substances. This process varies based on the origin of material being used. During the chemical hydrolysis, weak acids, such as acetic acid, citric acid, lactic acid, and inorganic acids, are commonly used. This process is used to break the

inter-strand cross-links of collagen and increase solubility of collagen (Schmidt et al., 2016). In addition, collagen is soluble in a salt solution. Salts such as sodium chloride, Tris hydroxymethyl aminomethane hydrochloride (Tris-HCl), phosphates, or citrates can be added to the acidic solution. The enzymatic hydrolysis is then performed by adding selected enzymes such as pepsin, trypsin, alcalase, collagenase, or pronase to the acidic solution (Schmidt et al., 2016). Many factors in this process, such as enzyme concentration, temperature, time, and pH, are adjusted depending on the collagen source to optimize the enzymatic activity. Most commonly used digestion methods are acid solubilization and pepsin solubilization for bovine collagen extraction (Ju et al., 2020).

2.1.1. Pepsin Digestion

Pepsin, a proteolytic enzyme that will be focused in this study, removes the helical ends of collagen (Ran & Wang, 2014). Collagen structure consists of three chains arranged in a triple helix structure, ending in a telopeptide region positioned on both ends of the chains. These terminals easily engage in covalent bonds, but can be cleaved off to produce acid soluble collagen with hydrogel forming properties. The main antigenic determinants are located in the telopeptides of collagen, which are removed through the pepsin treatment (Miyata et al., 1992). The resulting telopeptide-free molecules are also called atelocollagen (Hoshi et al., 2013). This cleavage reduces the antigenicity and immune activity of collagen, making it more applicable in in vivo biomedical applications. Once extracted, the atelocollagen is more soluble and possesses low immunogenicity and high biocompatibility comparing to untreated collagen (Li et al., 2018). When using pepsin, there is a direct relationship between pepsin activity and pH of the environment as shown in Figure 2.1.

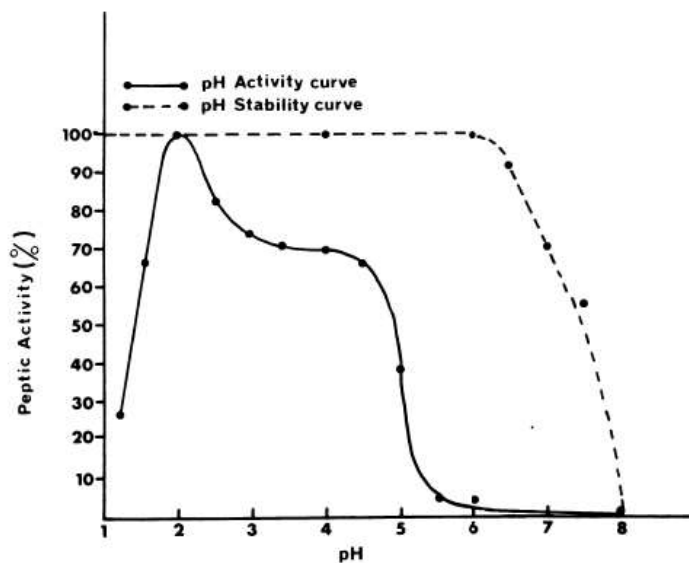


Figure 2.1. Pepsin activity based on pH (Piper & Fenton, 1965).

Pepsin becomes almost completely inactive once the environment pH reaches 7 (Piper & Fenton, 1965). During the fabrication of collagen-based scaffolds, pH is neutralized to deactivate the pepsin digestion process. These fibers must be further purified to remove any remaining impurities and to obtain a homogenous sample. For bovine tendons, pepsin soluble digestion yielded 10 times more collagen than acid soluble digestion (Zeugolis et al., 2008). In addition, acid solubilization does not cleave the collagen molecule of its telopeptide regions (Rahimi et al., 2020). Pepsin digestion therefore appears to be necessary for the production of atelocollagen, but no study has investigated the optimal pepsin-to-tendons ratio for bovine sourced collagen. A 1:10 (w/w) pepsin-to-tissue ratio is a commonly used for other species, such as emu skins (Nagai et al., 2015), and jellyfish (Khong et al., 2018). The optimal ratio of pepsin for bovine collagen extraction could be different given the high level of crosslinking of collagen in

bovine achilles tendons. Variations of pepsin ratio were conducted on bovine collagen extraction protocols. Bovine collagen at a w/w ratio of 1:10, 1.25:10, and 1.5:10 was used to determine the most effective and advantageous approach for yielding collagen solutions.

2.1.2. Bovine Collagen and Its Applications

There are several challenges that must be overcome in the extraction and purification of bovine collagen type I. One of the main challenges is the variability in the composition and quality of the raw bovine tissue, which can affect the efficiency and effectiveness of the extraction and purification processes. Additionally, the use of enzymes and other chemical agents in the extraction process can introduce impurities and alter the structural properties of the collagen. In this context, in the application of osteochondral repair, bovine collagen was the most promising source.

The overall goal of this experimentation is to collect a collagen containing solution that is usable for scaffold fabrication. It should also be noted that, the initial tendon weight to volume of acetic acid (w/v) ratio is a parameter that is manipulated across collagen source extractions. Although the molarity of acetic acid used (0.5 M) seems very consistent among protocols reported (Aukkanit & Garnjanagoonchorn, 2010; Khong et al., 2018; Nagai et al., 2015), their weight to volume (w/v) ratios vary from 1:10 (Aukkanit & Garnjanagoonchorn, 2010) to 1:100 (Khong et al., 2018) depending on the collagen sources. While bovine is the source, the tendon-to acetic acid ratio ranges from 1:5 to 1:20 (w/v) (Ju et al., 2020; Noorzai et al., 2020; Ran & Wang, 2014). This parameter affects the viscosity and homogeneity of the solution, so it was hypothesized that a solution with high viscosity decreases the efficiency of the enzyme digestion, thus leading to improper

cleavage of collagen molecule telopeptides and a lower yield of extracted atelocollagen. Another parameter that has also been studied is the location of extraction of the achilles tendon. The extraction differences between bovine and porcine tissues and genders have been investigated (Soroushanova et al., 2021). It was found that male bovine tendons possess the lowest yield of collagen. This was concluded that based on the amount of activity and mechanical loading variation between each species and gender, the crosslinking density of the collagen varies. The increase in mechanical loading of male bovine tendon results in an increase in the formation of collagen α -chain dimers (Kaku et al., 2016). In addition, local meat markets most commonly use male cattle for meat consumption, which have a higher crosslinking density compared to females (Soroushanova et al., 2021). As a result, the bovine achilles tendon were separated based on the compactness of the tendon tissue, the soft part being the superior region and the tough part being the inferior region. These locations are shown in Figure 2.2. For scaffold fabrication, we tried to collect as much of the superior region as possible.

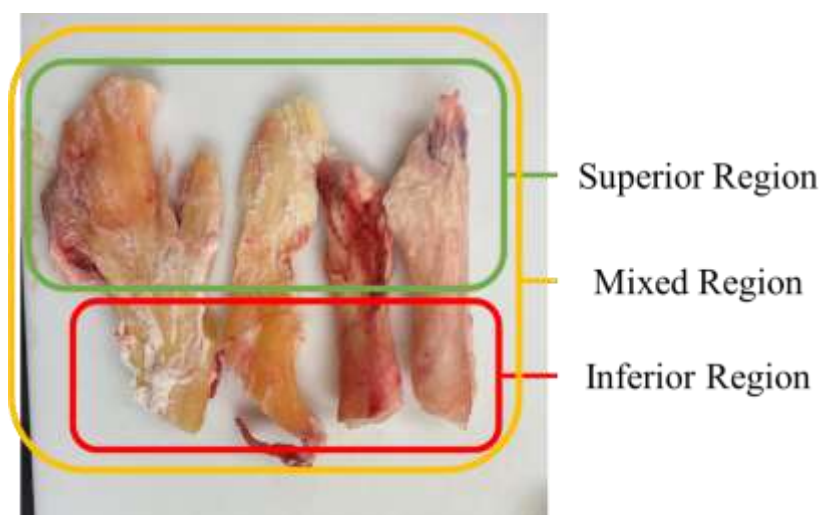


Figure 2.2. Bovine achilles tendon separation.

2.2. Methods and Materials

Bovine achilles tendons were purchased from Seaman's Cardinal Super Market in Athens, OH and stored at -18°C for less than 6 months. The tendons were mechanically separated from fats and loose areolar tissues, shown in Figure 2.3.a. Each region of the tendon was then separated based on superior and inferior locations of thus tendon. Such treated bovine tendons were flash frozen with liquid nitrogen, blended by the mean of an electric blender and rinsed with acetone to dissolve the remaining fat. The initial tendon weight was then measured and placed into 0.5 M acetic acid (A38-212 from Fisher Chemical) at initial tendon weight (g) to acetic acid volume (mL) ratios (w/v) of 1:40, 1:80, and 1:160 for 72 hours.

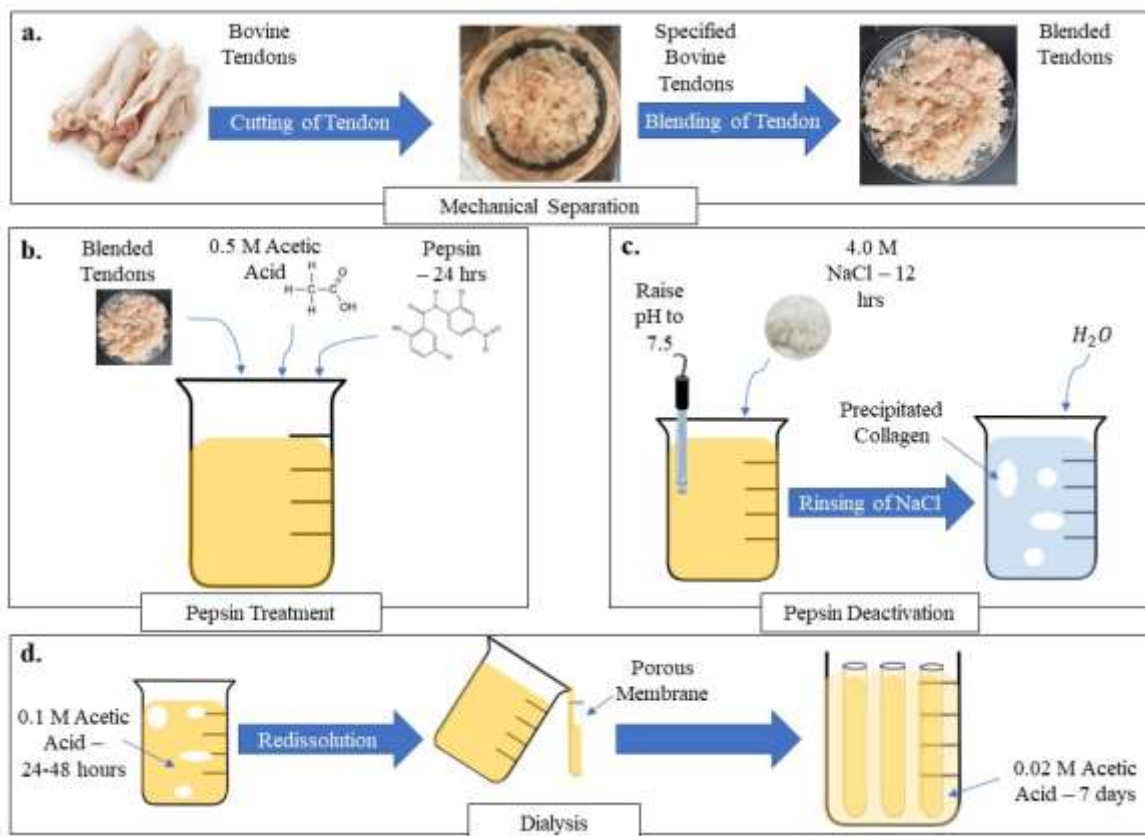


Figure 2.3. Extraction of bovine collagen. (a) Mechanical separation of bovine tendons. (b) Pepsin treatment. (c) Pepsin deactivation and salt bath. (d) Redissolution of collagen and dialysis.

2.2.1. Pepsin Digestion of Bovine Type I Collagen

Pepsin was chosen to digest bovine collagen. After 72 hours of immersion in acetic acid, pepsin (9001-75-6 from MP Biomedicals) was added to the acetic acid solution at a pepsin weight to tendon weight (w/w) ratio of 1:10, 1.25:10, or 1.5:10. The independent pepsin ratios along with their tendon weight to acetic acid volume (w/v) are shown in Table 2.1. The pepsin digestion was then initiated by stirring at 4°C for 24 hours as shown in Figure 2.3.b.

Table 2.1. Extraction protocols

Pepsin/Tendon Ratio (g/g)	Tendon/Acetic Acid Ratio (g/mL)	# of Trials
1:10	1:40	7
	1:80	7
1.25:10	1:40	3
	1:80	5
1.5:10	1:40	2
	1:80	3

2.2.2. Pepsin Deactivation and Salt Bath

Pepsin digestion was then terminated by centrifugating the collagen containing solution for 30 minutes at 25,000 x g relative centrifugal force (RCF) using a Thermo Scientific Sorvall Legend XT/XF series centrifuge (model 75004521). The supernatant was then collected, and the insoluble precipitate was removed. Figure 2.4 shows the comparison of solubilized vs. insolubilized collagen.

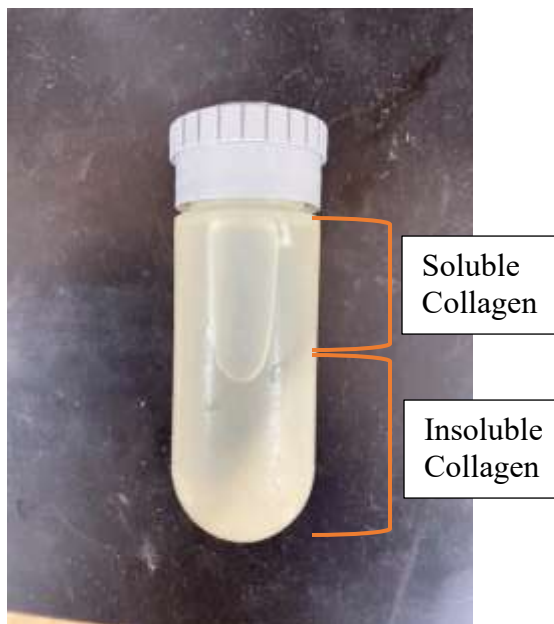


Figure 2.4. Pepsin treated collagen solution after initial centrifugation.

1 M Tris-HCL (BP152-1 from Fisher Bioreagents) was used to raise the suspension pH to 7.5 and deactivate the pepsin as shown in Figure 2.1. 4.0 M NaCl (7647-14-5, Fisher Chemical) was then added to the solution and left for 12 hours at 4°C with no stirring to promote collagen precipitation as shown in Figure 2.3.c.

2.2.3. Redissolution and Dialysis

After the 12-hour salt bath, the suspended collagen was then formed into pellets. The precipitated collagen was then rinsed with deionized water (DIW). This was performed by addition of DIW to the precipitated collagen solution and centrifugated at 25,000 x g RCF for 15 minutes. This process was repeated for 3 total times. The supernatant liquid was then discarded. The collagen pellets were then redissolved at 0.1 M acetic acid at 4°C for 24-48 hours to ensure all collagen was solubilized. Following the redissolution, the resulting insoluble pieces of collagen were discarded, and the solution underwent a

dialysis. The dialysis involved using porous cellulose bags (08-700-143 from Spectrum Laboratories) with 6-8 kDa molecular weight cut-off, allowing minerals and other components to withdraw from the collagen containing solution. The bags were sealed on both ends and set in 0.02 M acetic acid for 7 days, while replacing the acetic acid solution every 48 hours, as shown in Figure 2.3.d. The final collagen concentration was then measured by extracting 10 mL of solution (while stirring) and freeze drying (Labconco Corporation freeze dryer and tray dryer combo, models 710611100 and 794801000). The remaining dry tendon weight was then divided by the 10 mL of volume resulting in the collagen concentration in mg/mL. The yield collagen from extraction can be calculated in Equation 2.1 below:

$$\text{Yield \%} = \frac{\text{Collagen Concentration} \left(\frac{\text{mg}}{\text{mL}} \right) * \text{Final Solution Volume (mL)}}{\text{Initial Tendon Weight (mg)}} * 100\% \quad (2.1)$$

Due to the low yield of collagen extracted; the final solution was often too diluted and there is a need to freeze drying the collagen solution to increase the collagen concentration. This process prolonged the extraction process by approximately two weeks.

2.3. Results

The impact of pepsin and acetic acid concentrations on collagen yield is shown in Table 2.3. It is noted that the 1.5:10 pepsin/tendon ratio (g/g) resulted in the highest yield of collagen at $2.86 \pm 0.58\%$. While the 1.25:10 pepsin/tendon ratio (g/g) resulted in the lowest yield of collagen at $2.07 \pm 0.82\%$.

Table 2.2. Effect of pepsin and acetic acid concentrations on collagen yield

Pepsin/Tendon Ratio (g/g)	Tendon/Acetic Acid Ratio (g/mL)	Yield %
1:10	1:40 (n=7)	2.75 ± 0.85%
	1:80 (n=7)	2.46 ± 0.33%
1.25:10	1:40 (n=3)	2.21 ± 1.03%
	1:80 (n=5)	1.99 ± 0.79%
1.5:10	1:40 (n=2)	2.90 ± 0.85%
	1:80 (n=3)	2.84 ± 0.55%

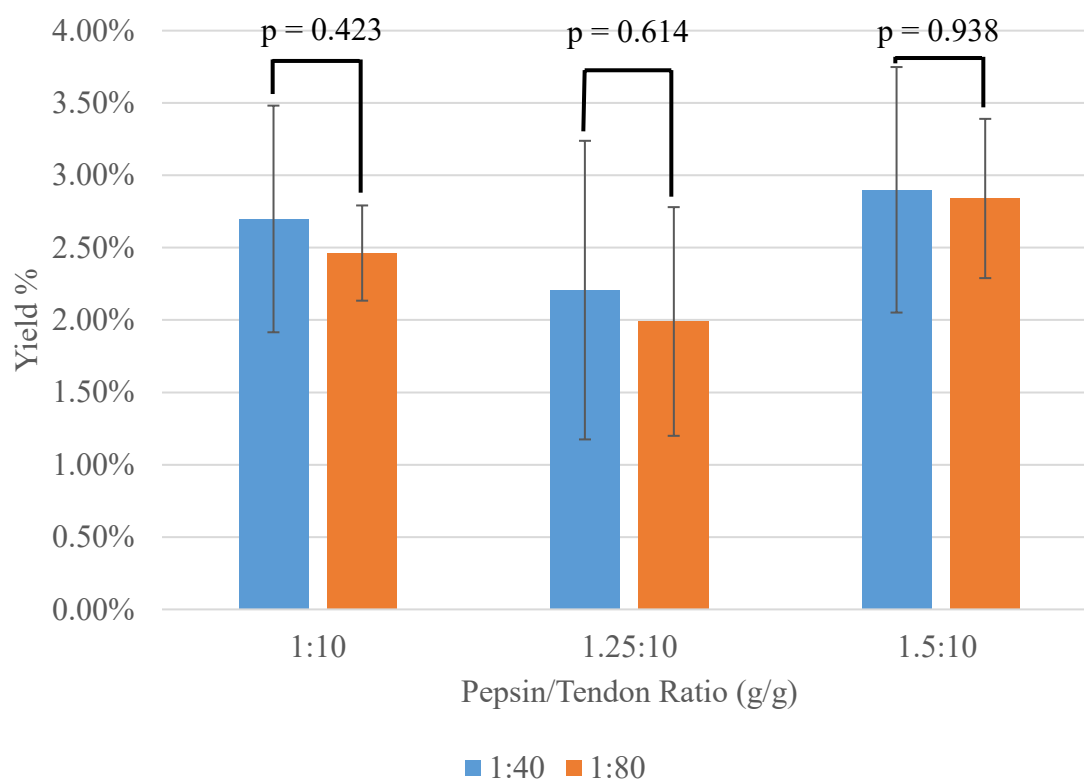
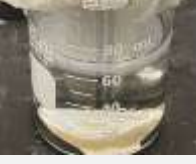


Figure 2.5. Pepsin/tendon ratio (g/g) and tendon/acetic acid ratio (g/mL) yield.

Regarding the tendon/acetic acid ratio (g/mL), there was no significant differences between the 1:40 and 1:80 ratios at each pepsin/tendon ratio (g/g) based on a confidence interval of 95%. A two-tail t-test was utilized in comparing each of the respected ratio at each pepsin/tendon weight ratio. The resulting p -values were calculated to be 0.423, 0.614, and 0.938 (two-tail) at each pepsin/tendon ratio (g/g) of 1:10, 1.25:10, and 1.5:10, respectively, which concludes $p > 0.05$, supporting that these datasets are not significantly different.

The results of each bovine tendon region are shown in Table 2.3. The superior region of tendon resulted in a yield of $2.66 \pm 0.59\%$, $2.00 \pm 0.86\%$, and $3.16 \pm 0.48\%$ for the 1:10, 1.25:10, and 1.5:10 pepsin/tendon weight ratios, respectively. As shown, the collagen containing solution resulted in proper gelation in the 1:10 and 1.25:10 groups for this region, but the 1.5:10 group lacked to form gel. The mixed region resulted in a yield of $2.36 \pm 0.54\%$, $2.65 \pm 0.08\%$ and $2.85 \pm 0.78\%$ for the 1:10, 1.25:10, and 1.5:10 pepsin/tendon ratios, respectively. By visual inspection, this region resulted in gelation of only half the adequate size for the 1:10 and 1.25:10 groups. Similar to the superior region, the 1.5:10 groups for this region did not show any sign of gelation. The inferior region resulted in a yield of $3.92 \pm 0.76\%$, $0.92 \pm 0.30\%$, and $1.43 \pm 0.33\%$ for the 1:10, 1.25:10, and 1.5:10 pepsin/tendon ratios, respectively. However, gelation only occurred in the 1.5:10 group, which is the opposite to the results observed in the previous two groups.

Table 2.3. Bovine tendon yields and their gelation capabilities.

Bovine Tendon Region	Pepsin/Tendon Ratio (g/g)	Yield %	Gelation Results
Superior Region 	1:10	2.66 ± 0.59% (n=7)	
	1.25:10	2.00 ± 0.86% (n=7)	
	1.5:10	3.16 ± 0.48% (n=2)	
Mixed Region 	1:10	2.36 ± 0.54% (n=6)	
	1.25:10	2.65 ± 0.08% (n=2)	
	1.5:10	2.85 ± 0.78% (n=2)	
Inferior Region 	1:10	3.92 ± 0.76% (n=2)	
	1.25:10	0.92 ± 0.30% (n=2)	
	1.5:10	1.43 ± 0.33% (n=3)	

2.4. Discussion

Optimization of bovine atelocollagen extraction has been investigated in this chapter. Bovine achilles tendon harvest region and pepsin-to-tendon ratio for collagen digestion were studied. Effects of these two parameters on collagen yield and hydrogel formation were investigated. An efficient and repeatable bovine collagen extraction protocol was established.

Collagen type I structure can be shown in Figure 2.6.a. The formation consists of 3 α chains that form a helix structure (Fratzl, 2008; Friess, 1998). Followed by a N-terminal and C-terminal regions named telopeptides on each end. Due to the antigenicity that is attributed to the telopeptide regions, cleavage of these regions is optimal for biomedical applications. Pepsin digestion was conducted to remove these regions and eliminate the collagen molecule's immunogenicity, as shown in Figure 2.6.b. This resulted in an atelocollagen molecule that has a positively charged surface, which increases the solubility and biomaterial processability (Holmes et al., 2017). Hydrogels (>90% water content materials) can then be formed from atelocollagen (Sarrigiannidis et al., 2021). Amines and carboxyl, the free functional groups of collagen, are used to create physical or chemical crosslinks (Ahn et al., 2013). These cross-links can be utilized to create hydrogels, as shown in Figure 2.6.c. However, noncleaved telopeptide regions promote fibrillogenesis between collagen molecules. Fibrillogenesis is the process of telopeptides inducing covalent bonds or crosslinks between opposing collagen molecules (Kuznetsova & Leikin, 1999). This bonding can only occur between a telopeptide terminal and an opposing collagen triple helix region (Abou Neel et al., 2013; Knott & Bailey, 1998). These bonds

create a staggered bridge between collagen fibrils as shown in Figure 2.6.d, but they do not gelate. This was found to be an occurrence in the gelation of the mixed and inferior regions at both 1:10 and 1.25:10 pepsin/tendon (g/g) ratio groups, as shown in Table 2.3.

Denaturation of collagen is the process of hydrogen bonds breaking between the 3 α chains, resulting in a separated coiled form, as shown in Figure 2.6.e. (León-López et al., 2019). These denatured chains can then be hydrolyzed by proteolytic enzymes, which result in hydrolyzed collagen, shown in Figure 2.6.f. The hydrolyzed collagen is defined as peptides that have a low molecular weight of 3-6 KDa (Hong et al., 2017; Ketnawa et al., 2017; Thuanthong et al., 2017). A setback with hydrolyzed collagen is scaffold formation is not feasible by itself (León-López et al., 2019). This is in agreement with our results of the 1.5:10 pepsin/tendon (g/g) ratio groups for the superior and mixed region groups. As shown in Table 2.3, each of these groups did not gelate at all, resulting in small free collagen peptides. This was caused by excessive pepsin treatment, which completely denatured the collagen molecules.

For superior region, the yield for both the 1:10 and 1.25:10 groups was a mixture of collagen fibrils and primarily atelocollagen which ultimately led to gelation. This is due to proper cleavage of the telopeptide regions, which allowed for the self-assembly of collagen molecules (Lin et al., 2019). Although the yield for 1:10 is higher than that of the 1.25:10 group, but it contains a higher proportion of collagen fibrils, so the gel formed is less sturdy. In the case of the 1.5:10 group, the collagen was completely denatured, due to the excessive enzyme digestion, and it turned into low molecular weight peptides, which did not gelate at all.

For the inferior region, the collagen is more crosslinked compared to that of the superior region. Although the yield was still a mixture of collagen fibrils and atelocollagen for both the 1:10 and 1:25:10 groups, but the proportion of atelocollagen is much lower compared to those of the superior region. As a result, a thin layer of gel was observed for both groups, but most of the yields were collagen fibrils, which did not form gel. A thinner gel layer was observed for the 1.25:10 group compared to the 1:10 group, indicating more atelocollagen was formed in the 1.25:10 group. When the pepsin concentration increased to 1.5:10, more atelocollagen was formed in this highly crosslinked collagen region. As a result, gelation was observed. Still, the gel was less sturdy than that of the 1.25:10 group from the superior region, but similar to that obtained from the 1:10 group from the superior region.

For the mixed region, the yield result is between the superior and the inferior regions. Collagen gels were formed for both the 1:10 and 1.25:10 groups, but they only filled part of the container. These groups contained a yield mixture of collagen fibrils and atelocollagen. In the case of the 1.5:10 group, the yield is a mixture of collagen fibrils, atelocollagen and denatured collagen. As a result, we see a very thin layer of gel formed on the surface of the solution and a mixture of collagen fibrils and low molecular weight peptides at the bottom of the solution. Table 2.4 summarizes the collagen yield collected from these three regions.

Table 2.4. Impact of collagen collected region on collagen yield composition.

Bovine Tendon Region	Pepsin/Tendon Ratio (g/g)	Yield %	Yield composition
Superior Region	1:10	2.66 ± 0.59% (n=7)	Collagen fibrils and atelocollagen
	1.25:10	2.00 ± 0.86% (n=7)	Atelocollagen
	1.5:10	3.16 ± 0.48% (n=2)	Atelocollagen and denatured collagen
Mixed Region	1:10	2.36 ± 0.54% (n=6)	Collagen fibrils and atelocollagen
	1.25:10	2.65 ± 0.08% (n=2)	Collagen fibrils and atelocollagen
	1.5:10	2.85 ± 0.78% (n=2)	Collagen fibrils, atelocollagen, and denatured collagen
Inferior Region	1:10	3.92 ± 0.76% (n=2)	Collagen fibrils and atelocollagen
	1.25:10	0.92 ± 0.30% (n=2)	Collagen fibrils and atelocollagen
	1.5:10	1.43 ± 0.33% (n=3)	Collagen fibrils and atelocollagen

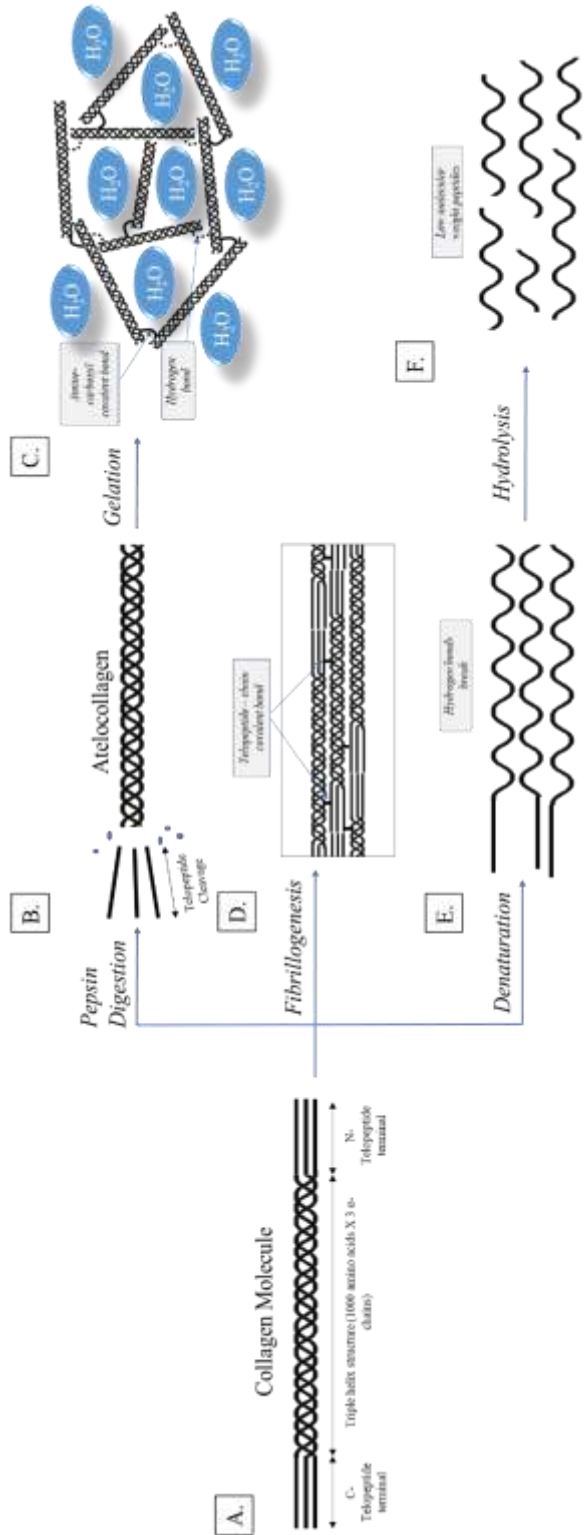


Figure 2.6. (a) Type I collagen molecular structure, (b) Atelocollagen formation through pepsin digestion, (c) Gelation of atelocollagen, (d) Fibrillogenesis formation of collagen, (e) Denaturation of collagen, and (f) Hydrolysis to collagen peptides (Cavelier et al., 2023).

The bovine tendon regions each varied in gelation capability. This experimentation was conducted based on the mechanical differences throughout the bovine achilles tendon. The anatomy of the achilles tendon is shown in Figure 2.7.

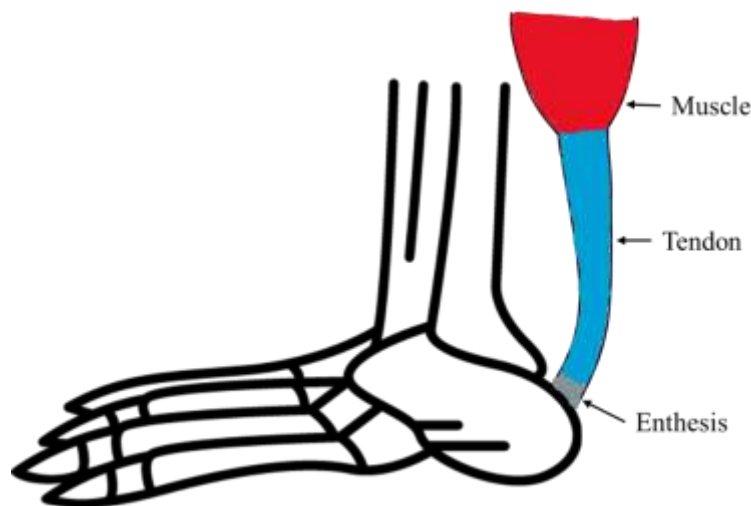


Figure 2.7. Achilles tendon anatomy.

The mineral content, collagen orientation, protein gradient, and mechanical properties from the tendon to the bone vary. The tendon-bone interface, also known as the enthesis, consists of mainly mineralized collagen (Ellingson et al., 2022). The closer to the point of insertion, collagen becomes more ossified, less aligned, and aggrecan content is greater (Thomopoulos et al., 2003). As the tendon reaches this region, an increase to deformation and energy absorption results in an overall tougher tissue (Deymier et al., 2017). This led to determine the level of collagen crosslinking increases the closer to the insertion site. Although, there is a gap of knowledge in this area due to the testing of the physiological mechanics of the enthesis. This takeaway correlates with the enzymatic digestion efficiency, where the cross-linking density of the inferior region (closer to bone) was

greater compared to the superior region (closer to muscle). This led to our results of the inferior region, whereas an increase in the pepsin/tendon weight ratio led to proper enzymatic cleavage of telopeptides. This ultimately led to hydrogel formation in the 1.5:10 group of the inferior region, shown in Table 2.3. Whereas a reduced pepsin/tendon weight ratio was needed in the superior region for proper enzymatic digestion. Shown in the 1:10 and 1.25:10 groups of the superior region in Table 2.3.

The quantity of hydroxyproline is often an indicator of the structural stability of collagen molecules (Xu et al., 2019). A study on the extraction of collagen from human perirenal adipose tissue indicates that pepsin digestion can be utilized to quantify the amount of total protein concentration and hydroxyproline concentration (Lee et al., 2022). It was found that between a range of 0.5-2.0% pepsin/collagen (w/w), the 1.0% group did not have the greatest protein yield, but did have the greatest hydroxyproline concentration. It was concluded that this pepsin concentration was optimal for yielding the highest atelocollagen extraction, while still preserving the collagen molecule. Similarly, it was found in our study that collagen extracted from the 1:10 and 1.25:10 pepsin/tendon ratios batches from the superior region and the 1.5:10 pepsin/tendon ratio batches from the inferior region formed gel network. It was also noted that the rigidity of gel in 1.25:10 pepsin/tendon ratio of the superior region was more stable than the other 1.5:10 pepsin/tendon ratio of the inferior region and 1:10 pepsin/tendon ratio of the superior region groups. This correlates with a greater amount of atelocollagen and hydroxyproline that allowed for higher collagen fibril assembly while maintaining molecule stability.

After manipulation of the tendon/acetic acid ratio, the gelation results did not vary based on this parameter. Although the yield of collagen extracted was unsteady, this parameter is believed to be negligible to atelocollagen content. As the resulting gel was consistent based upon the pepsin/tendon ratio in spite of the tendon/acetic acid ratio.

2.5. Conclusion

A study was conducted to determine the optimal parameters for extraction of bovine collagen. Due to the nature of collagen, the pepsin digestion process could not completely cleave the telopeptide region of every collagen molecule. Optimized parameters, including the use of superior region of the bovine achilles tendon and a pepsin/tendon ratio (g/g) of 1.25:10, have been determined. The inferior region of the achilles tendon is highly crosslinked, so it is difficult to be cleaved by pepsin. In addition, it was found that the optimal pepsin-to-tendon ratio not only properly cleaves the telopeptide regions but also maintain the molecular stability of collagen.

Chapter 3 - Fabrication of Collagen Hydroxyapatite Lamellar Scaffold

3.1. Introduction

Collagen hydroxyapatite scaffolds exhibited promising results for bone repair and regeneration due to their composition similar to native tissue. Bone is naturally composed of hydroxyapatite $[\text{Ca}_{10}(\text{PO}_4)_6(\text{OH})_2]$, which makes these scaffolds substantially advantageous compared to other solutions in osteochondral repair (Boskey & Robey, 2013). The fabrication of collagen hydroxyapatite scaffolds involves the use of a series of salts to create a modified-simulated body fluid (m-SBF) and hydroxyapatite deposition. pH fluctuation in the solution would initiate the assembling of atelocollagen molecules into a gel network, while allowing apatite to precipitate on the collagen (Xia et al., 2014). A direction-controlled freezing approach was used to orient the collagen fibers in preferred directions and create a layered structure, thus mimicking the structure of the deep and osseous zones in articular cartilage. This unidirectional freezing promoted ice growth in one direction resulting in an anisotropic pore structure (Xia et al., 2013). This lamellar structure has previously shown advantages of osteogenesis and in vivo bone regeneration (Yu et al., 2020).

3.1.1. Biocompatibility

Studies have been conducted regarding the biocompatibility of collagen hydroxyapatite scaffolds. In aqueous media, hydroxyapatite has shown to possess a lower degradation rate and a higher stability at a 4.2-8 pH among the calcium phosphates (Kumar et al., 2019), making it a highly studied compound for bone tissue repair. Collagen has shown advantages of controlled degradation rate, biocompatibility, and growth and assembly of

hydroxyapatite crystals in a fiber network (Filip Ionescu et al., 2022; Muthukumar et al., 2018). It has been noted that collagen mineralized scaffolds support bone marrow mesenchymal cells (BMSCs) and fresh bone marrow cells proliferation and adhesion (Filip Ionescu et al., 2022; Yu et al., 2020).

3.1.2. Porosity & Pore Size

The porosity and pore size of collagen-based scaffolds has been reported to be ideal for promoting bone cell growth. Pore sizes in the range of 50 – 500 μm are ideal for supporting cell viability and mechanical properties of the scaffold (Xia et al., 2013). These variables can be controlled by different characteristics. A study on biomimetic collagen-apatite scaffold with a multi-level lamellar structure was conducted by Xia et. al. An increase in self-compression time on the apatite/collagen gel led to an increase in collagen fibrillar density. During this process, water was squeezed out of the material because of the effect of pressure exerted by the weight of the gel. With an increase in collagen fibrillar density ($\rho_{collagen}$), the porosity of the scaffold decreased (Xia et al., 2013). In general, as the porosity of a scaffold increases, the cell viability increases. In contrast, as the porosity increases, the mechanical properties of the scaffold decrease (Zhang & Cooper, 2007). The porosity of a scaffold is described by Equation 3.1 (Al-Munajjed et al., 2009):

$$Porosity = 1 - \frac{m_{scaffold}}{V_{scaffold}} * \left(\frac{\omega_{collagen}}{\rho_{collagen}} + \frac{\omega_{apatite}}{\rho_{apatite}} \right) \quad (3.1)$$

Where the mass and volume of each scaffold is represented as $m_{scaffold}$ and $V_{scaffold}$.

The weight ratio of collagen ($\omega_{collagen}$) and apatite ($\omega_{apatite}$) are measured values. The

densities of apatite (ρ_{apatite}) and collagen (ρ_{collagen}) were referenced from a past study to be 3.16 and 1.32 g/cm³, respectively (Xia et al., 2014).

3.2. Methods and Materials

Bovine collagen solution, of at least 3.0 mg/mL in concentration, was used to fabricate a lamellar scaffold. A modified-simulated body fluid consisting of NaCl (S271-500 from Fisher Chemical), CaCl (C614-500 from Fisher Chemical), NaHCO₃ (S233-500 from Fisher Chemical), K₂HPO₄ (16788-57-1 from Acros Organics) and MgCl₂ (M35-500 from Fisher Chemical) was mixed with DIW and added to the collagen solution in determined proportions. A buffer of HEPES, 4-(2-hydroxyethyl)-1-piperazineethanesulfonic acid, (J16926-30 from Thermo Scientific) was also added. Once mixed, the pH was raised to 7 by dropwise addition of approximately 2-3 mL of NaOH (SS266-1 from Fisher Chemical) monitored by a pH probe (13620183A from Fisher Scientific). The solution then sat at room temperature for 1 hour. This process is shown in Figure 3.1.a.

3.2.1. Gelation, Self-Compression, and Freeze Drying

After sitting at room temperature for 1 hour, the solution was then kept at 37°C for 12 h during which gel formation occurred as shown in Figure 3.1.b. The gel held its integrity during manipulation and composed at least 90% of the beaker's volume. It was then followed by a self-compression to decrease the volume fraction of liquid and align the fibers in the direction of water evacuation. The self-compression involved the lid of a petri dish being applied from above, to pressurize the gel and promote evacuation of the excess fluid from small holes at the bottom of the petri dish. After 15 minutes, the gel would reach a thickness of approximately 20 mm as shown in Figure 3.1.c and was radially frozen in

the freeze dryer. As shown in Figure 3.1.d, insulating foams were placed on the top and bottom surfaces of the gel, allowing the gel to freeze radially. It took approximately 12 to 24 hours at -40°C to freeze the scaffold. Following the freezing, a vacuum (0.010 mbar) was initiated to lyophilize the ice and form the scaffold. The length of time required for vacuuming varied depending on the overall size of the scaffold. Generally, the scaffold needed 3 to 7 days to completely freeze dry completely.

3.2.2. Scaffold Crosslinking

Once completely dried, the resulting lamellar scaffold (shown in Figure 3.1.d.) was crosslinked using MES Monohydrate buffer (MFCD00149409 from MP Biomedicals), with EDC (1-Ethyl-3-[3dimethylaminopropyl] carbodiimide HCL) (22980 from Thermo Scientific), and NHS (A10312 from Alfa Aesar) with DIW. The solution was then titrated to pH=5 using drop wise addition of HCl (SA448-1 from Fisher Chemical). The scaffold was then placed in the solution for 4 hours after pressing it with a disinfected spatula to ensure all air bubbles were evacuated from the inner pores. After 4 hours, the scaffold was immersed in 5% glycine (G48-500 from Fisher Chemical) to DIW (w/v) for 12 hours. After sitting in 5% glycine, the scaffold was rinsed thrice, freeze dried and stored at 4°C .

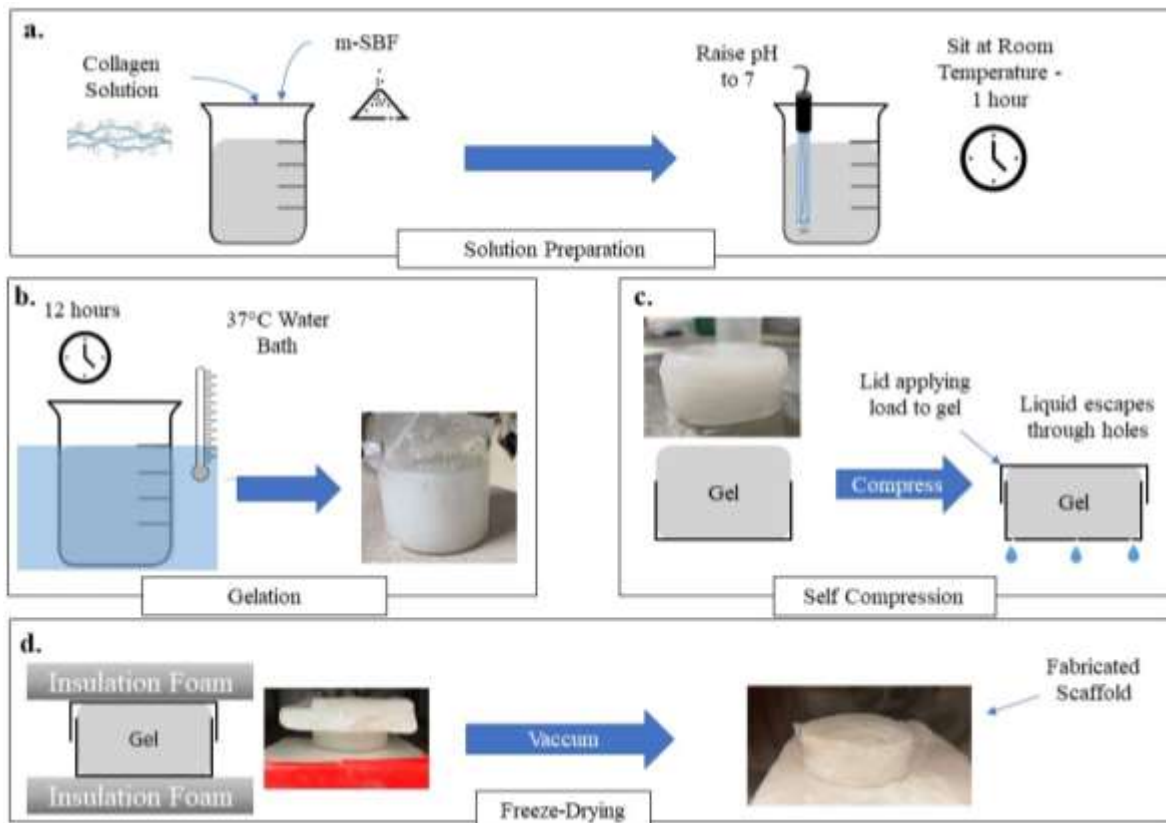


Figure 3.1. Fabrication of collagen-hydroxyapatite lamellar scaffold. (a) Collagen-mineral solution preparation. (b) 37°C water bath and gelation of the suspension. (c) Self-compression. (d) Radial freezing and freeze-drying.

3.2.3. Scaffold Characterization

3.2.3.1. SEM and EDS

The cross sections of the scaffold were observed using scanning electron microscopy (SEM; JEOL JSM-639OLV) and the elemental content of the scaffold was determined using energy-dispersive X-ray spectroscopy (EDS; LA 6510) affiliated with the SEM. The elemental compositions of calcium (Ca), phosphorous (P), sodium (Na), chloride (Cl) and carbon (C) were analyzed.

3.2.3.2. FTIR

The surface functional groups of the scaffold were characterized using Fourier transform infrared spectroscopy (FTIR; Perkin Elmer Spectrum 65 FT-IR) with an attenuated total reflection unit (ATR; SensIR Technologies, 071-1514) over a range of 4000–500 cm^{-1} .

3.2.3.3. XRD

The phase composition of the scaffold was examined using X-ray diffraction (XRD; Rigaku MiniFlex 600) at a scan rate of $1^\circ/\text{min}$ and a step size of 0.02° .

3.2.3.4. TGA

The mineral content in the scaffold was measured using thermogravimetric analysis (TGA; TA Instruments Q500) over the range from room temperature to 1000°C with a heating rate of $10^\circ\text{C}/\text{min}$ and flow rate of $90\text{ mL}/\text{min}$ in air.

3.3. Results

The scaffold size before undergoing the crosslinking process is shown in Figure 3.2.a. The resulting scaffold exhibited a lamellar structure visible by eye prior to crosslinking. The scaffold measured roughly 35-40 mm in diameter, for a 66 mL initial suspension, as shown in Figure 3.2.b. The final thickness measured approximately 3 mm, which corresponds to a decrease of the initial thickness of approximately 65%, as shown in Figure 3.2.c and 3.2.d.

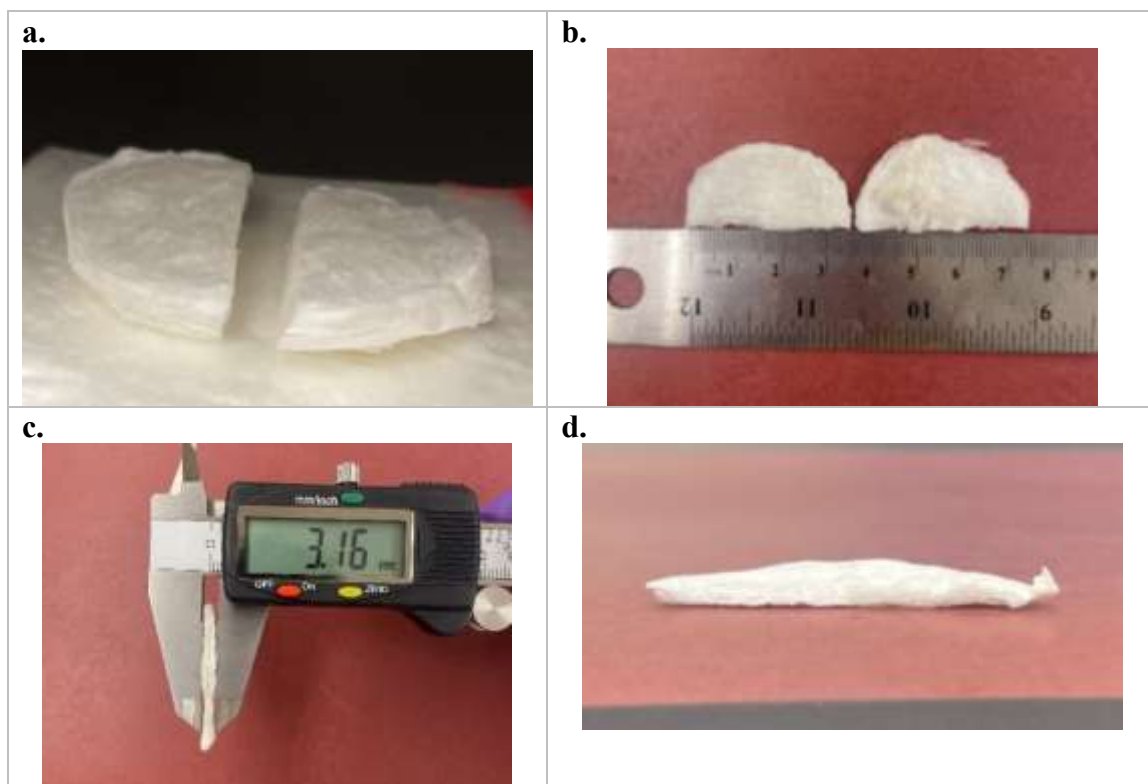


Figure 3.2. Collagen hydroxyapatite lamellar scaffold. (a) Scaffold before crosslinking process. (b) Scaffold after crosslinking process. (c) Thickness of scaffold after crosslinking. (d) Lamellar structure of scaffold.

The effect of pepsin concentration on scaffold fabrication using the collagen collected from the superior region is listed in Table 3.1. At a pepsin to tendon ratio of 1:10 (g/g), the success rate of scaffold formation was 66.7%, but the success rate increased dramatically (100%) when the ratio increased to 1.25:10. However, when the ratio was further increased to 1.5:10, no scaffolds were formed. Still, at the same pepsin to tendon ratio, the success rate of the collagen collected from the superior region is constantly higher than those collected from the mixed region.

Table 3.1. Scaffold attempts based on pepsin/tendon ratios of superior region collagen.

Pepsin/Tendon Ratio (g/g)	Successful Scaffolds	Unsuccessful Scaffolds
1:10	2 ; (66.6%)	1 ; (33.3%)
1.25:10	4 ; (100%)	0 ; (0%)
1.5:10	0 ; (0%)	2 ; (100%)

The effect of pepsin concentration on scaffold fabrication using the collagen collected from the inferior region is listed in Table 3.2. At a pepsin to tendon ratios of 1:10 and 1.25:10 (g/g), no scaffolds were formed. However, when the ratio is further increased to 1.5:10, every scaffold was formed.

Table 3.2. Scaffold attempts based on pepsin/tendon ratios of inferior region collagen.

Pepsin/Tendon Ratio (g/g)	Successful Scaffolds	Unsuccessful Scaffolds
1:10	0 ; (0%)	2 ; (100%)
1.25:10	0 ; (0%)	1 ; (100%)
1.5:10	2 ; (100%)	0 ; (0%)

The effect of pepsin concentration on scaffold fabrication using the collagen collected from the mixed region is listed in Table 3.3. At a pepsin to tendon ratio of 1:10 (g/g), the successful rate of scaffold formation was only 20%, but the successful rate increased to 50% when the ratio increased to 1.25:10. However, when the ratio is further increased to 1.5:10, none of the scaffolds were formed.

Table 3.3. Scaffold attempts based on pepsin/tendon ratios of mixed region collagen.

Pepsin/Tendon Ratio (g/g)	Successful Scaffolds	Unsuccessful Scaffolds
1:10	1 ; (20%)	4 ; (80%)
1.25:10	1 ; (50%)	1 ; (50%)
1.5:10	0 ; (0%)	1 ; (100%)

3.3.1. Characterization of Mineralized Collagen Lamellar Scaffolds

The scaffold was observed using scanning electron microscope (SEM) at a magnification of x40 and x75, respectively, as shown in Figure 3.3. A clear lamellar structure was observed in both images, and each lamella is composed of multiple mini-lamellae. The interlamellar distance of two adjacent lamellae was measured using the ImageJ software of the 2D images. It was found that the average distance was measured to be $162.4 \pm 32.97 \mu\text{m}$.

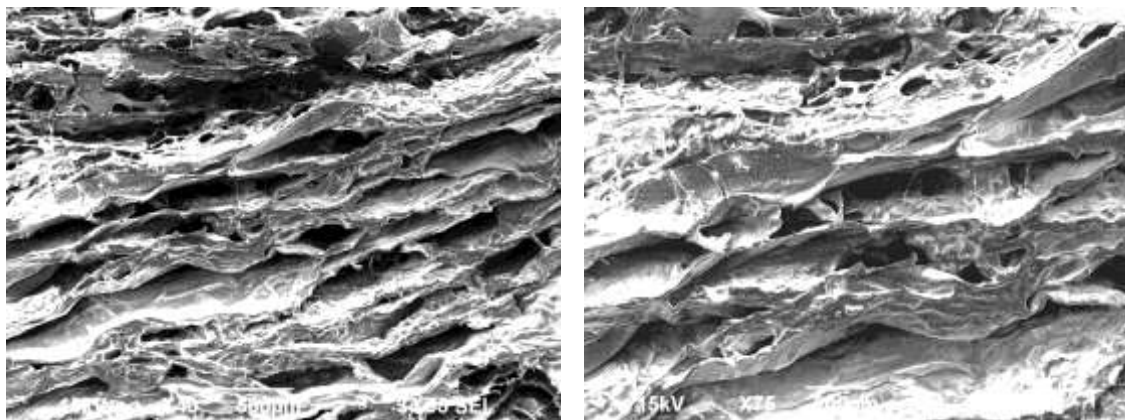


Figure 3.3. SEM images of a lamellar scaffold imaged at two different scales: (a) x40 and (b) x75.

An elemental analysis was also performed on the scaffold using energy dispersive spectroscopy, as shown in Figure 3.4. Notable elements found include calcium (Ca), phosphorous (P), sodium (Na), chloride (Cl) and carbon (C). Ca composed 1.71% of the atom percentage, P composed of 1.09% of the atom percentage, Na composed 2.77% of the atom percentage, Cl composed 1.23% of the atom percentage, and C composed of 64.53% of the atom percentage. The calculated Ca/P ratio of the scaffold was found to be 1.57, which is slightly lower than the Ca/P ratio of stoichiometric hydroxyapatite, 1.67. Besides the above elements, Mg and K were also observed. Both elements are key elements used in simulated body fluid for precipitating apatite onto collagen fibers.

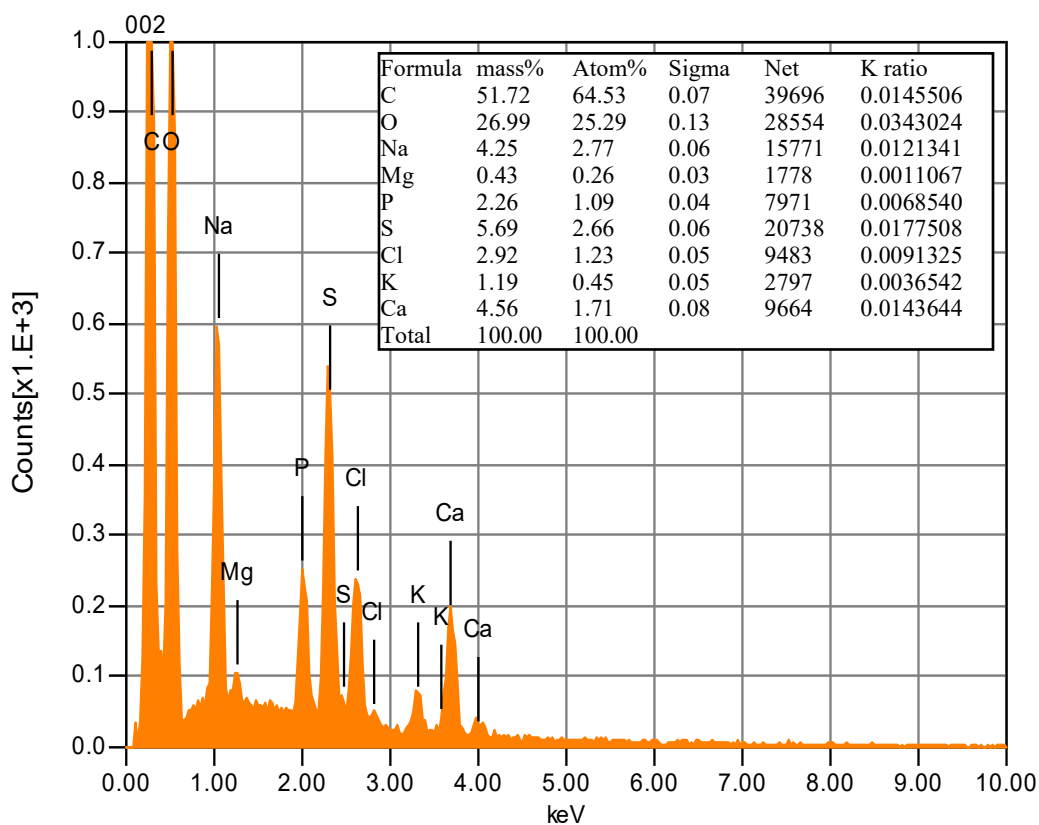


Figure 3.4. Elemental analysis of collagen hydroxyapatite lamellar scaffold.

Fourier-transform infrared (FTIR) spectroscopy was also used to examine the surface functional groups of the resulting scaffolds, as shown in Figure 3.5. The notable peaks labeled PO₄, Carbonate, amide I, amide II, and amide III were labelled in comparison to a study performed on collagen-hydroxyapatite lamellar scaffolds (Yu et al., 2020).

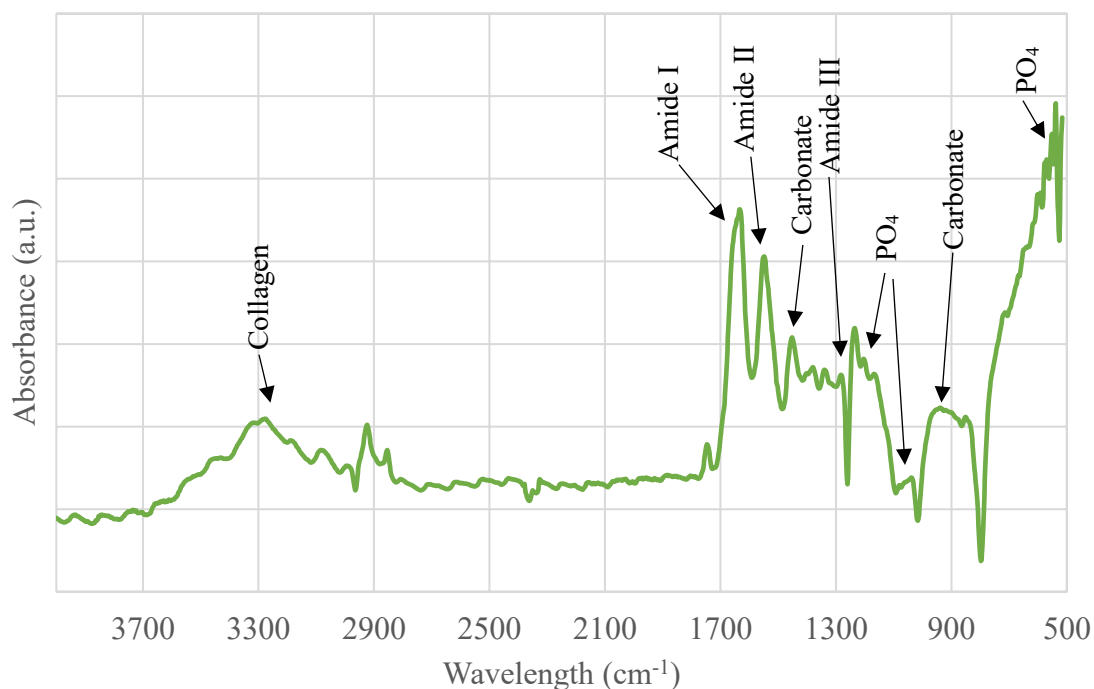


Figure 3.5. FTIR spectra of collagen hydroxyapatite lamellar scaffold with specific peaks.

In the XRD analysis, resulting scaffolds can be shown in Figure 3.6. It was found that a broad peak occurred at approximately 20°, which is attributed to collagen. An additional peak was noted at 31.7-32.5°, which is associated with the formation of apatite based on previous studies (Xia et al., 2014; Xia et al., 2013).

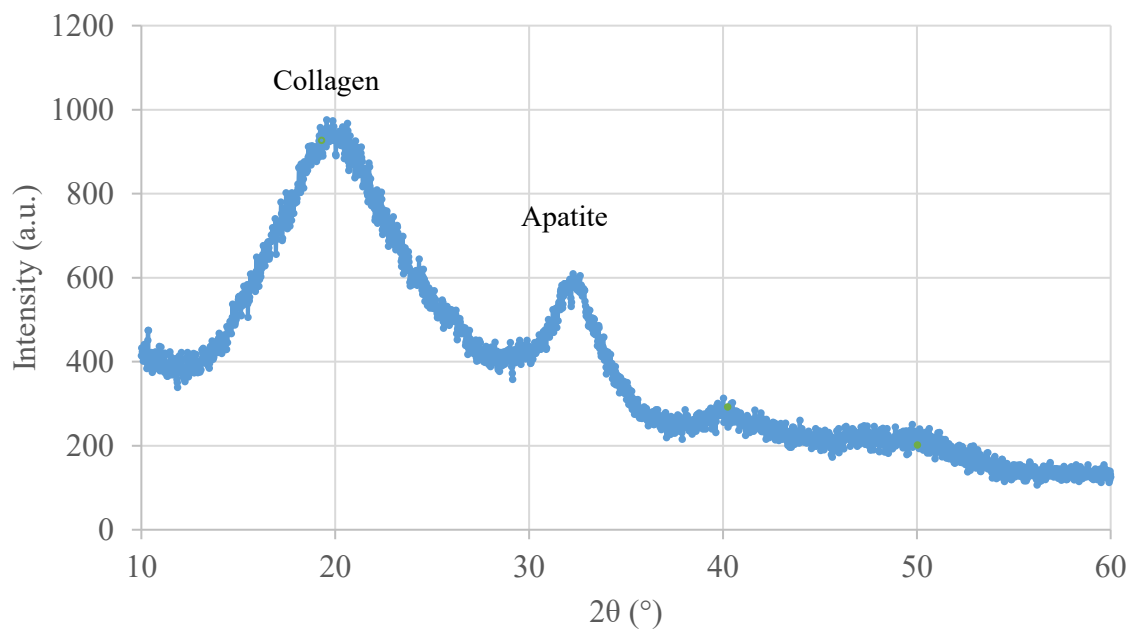


Figure 3.6. XRD of a mineralized collagen lamellar scaffold.

TGA analysis of the scaffold is illustrated in Figure 3.7. As shown in Figure 3.7, there is approximately 10% weight loss between room temperature and 210°C, which was mainly attributed to the removal of physically absorbed water by scaffolds. In comparison, the weight loss occurred between 210 and 580 °C mainly corresponded to the decomposition of collagen molecules, yielding approximately 15 wt% solid.

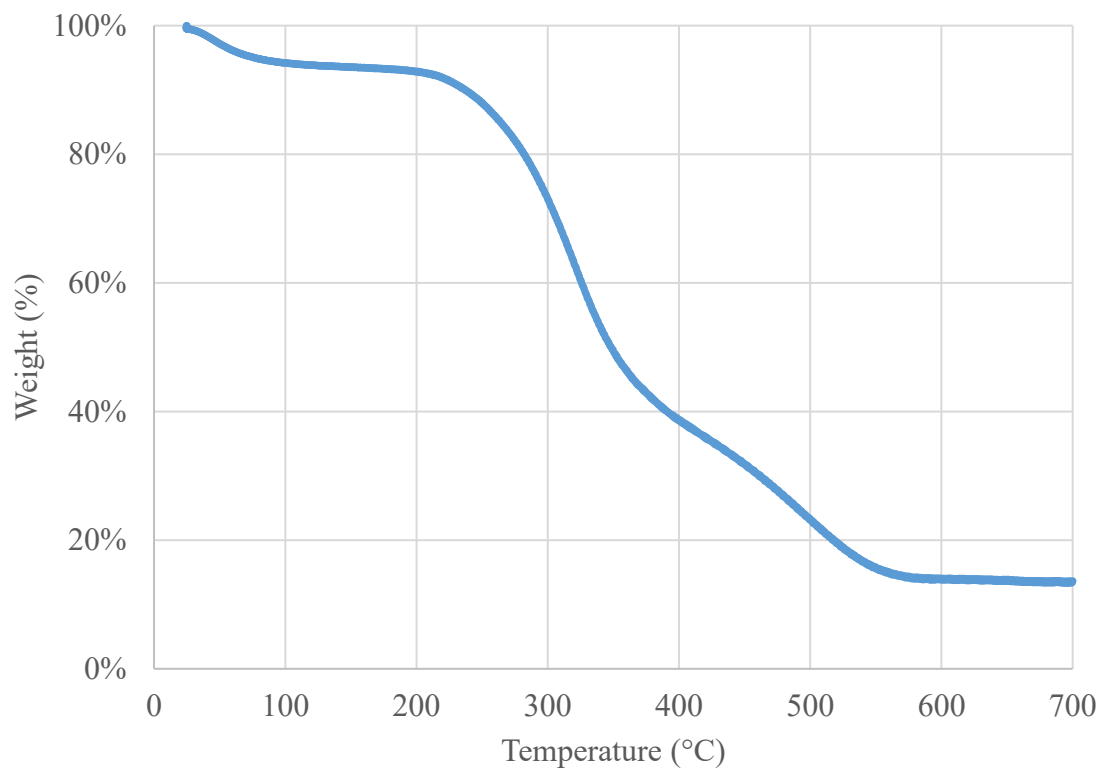


Figure 3.7. TGA of collagen hydroxyapatite lamellar scaffold.

3.4. Discussion

Visual inspection and SEM observation indicate that a lamellar hydroxyapatite collagen scaffold has been successfully created. The lamellar structure results from the lyophilization of the dendritic ice that grew align the collagen fibers and propagated parallel to the insulation foams (Xia et al., 2014). This lamellar structure mimics the collagen arrangement of the deep and osseous zones of osteochondral tissue. A schematic shows the process of lamellar scaffold formation, as shown in Figure 3.8.

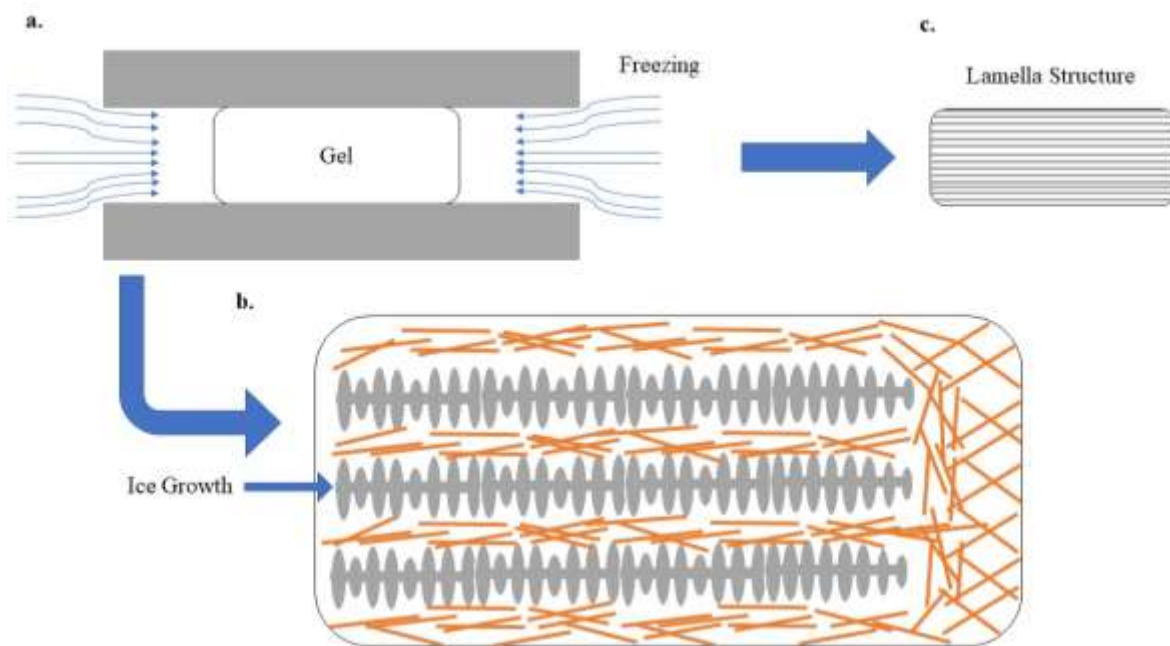


Figure 3.8. (a) Radial freezing of hydrogel. (b) Dendritic ice growth during directional freezing forces collagen fibers to arrange along a preferred direction. (c) Resulting scaffolds exhibit a lamellar structure mimicking the collagen arrangements in superficial and deep zones of cartilage tissue.

As shown in Figure 3.8.a, the foam insulators are placed on the top and bottom surfaces of the mineralized collagen gel, which allows for the unidirectional ice growth as shown in Figure 3.8.b. Although no *in vivo* or *in vitro* studies were conducted, it has been found that the lamellar structure provides greater osteogenesis capability compared to cellular structured collagen/apatite scaffolds (commercial and in-house) (Yu et al., 2020). In the study by Yu et al. (Yu et al., 2020), it was found that osteogenesis took place within collagen hydroxyapatite lamellar scaffolds *in vitro* using bone marrow stromal cells (BMSCs), along with *in vivo* bone regeneration within mice calvarial area.

A crucial aspect of mimicking biological systems is the directed growth of hydroxyapatite (Palmer et al., 2008). While bone consists of 30% organics (collagen,

glycoproteins, proteoglycans, and sialoproteins) and 70% minerals (primarily nanoscale hydroxyapatite crystals), this makes for a promising material in bone regeneration and repair (Olszta et al., 2007). The FTIR, XRD, SEM elemental analysis, and TGA all indicate hydroxyapatite has formed within the scaffold. In the XRD spectra, it can be seen in Figure 3.6 that the peak between $2\theta=31.7-32.5^\circ$, corresponds to the apatite that is poorly crystallized which resembles the carbonized hydroxyapatite in bone (Marelli et al., 2010). The EDS analysis successfully identified calcium (Ca) and phosphorous (P), at a Ca/P ratio of 1.57. Hydroxyapatite at its pure form contains 39.68% Ca and 18% P which results in a Ca/P ratio equal to 1.67 (Boskey, 2007; Ramesh et al., 2008). Our EDS result indicates CaP was successfully precipitated in the scaffold, and such formed CaP has a slightly lower Ca/P ratio, 1.57. Combining the results from EDS and XRD, calcium-deficient hydroxyapatite may have formed in the composite scaffold. Nevertheless, EDS is a relatively fast approach for elemental analysis, which provides a rough measure of elemental ratio of Ca/P. For a more accurate analysis, inductively coupled plasma mass spectrometry (ICP-MS) is generally used. Elemental analysis also indicates that some other elements, such as Na, K, Mg and Cl, still exist in the final scaffold, indicating more rinses are needed before these scaffolds can be used for in vitro and in vivo applications. There is also a possibility that some K and Mg substituted some Ca in hydroxyapatite and formed K- and Mg-containing hydroxyapatite. Both Ca and P in hydroxyapatite are easily substituted by other elements (Dey & Pal, 2009). A high percentage of C was also detected, which is contributed to the collagen composition. TGA was used to determine the makeup of mineralization within the scaffold. The weight loss of approximately 10% at 200°C was

contributed to evaporation of water. While the loss between 240-600°C, was a result of the collagen being decomposed (Yu et al., 2020). This resulted in a ~15 wt% residual of solid within the scaffold. This value is lower than previous studies due to the sourcing from bovine. Rat tail, a commonly used source of collagen, can form scaffolds at collagen solution concentrations of 0.5-3 mg/mL (Dey & Pal, 2009; Liu et al., 2000; Xia et al., 2013). Whereas, bovine needs a concentration of 3-4 mg/mL to properly form a scaffold. The increase of collagen concentration is inversely proportional to the amount of apatite deposition in the scaffold (Xia et al., 2013). Combining with the results from XRD, FTIR, and TGA, it is believed that the residual is calcium-deficient hydroxyapatite.

3.5. Conclusion

Overall, hydroxyapatite collagen lamellar scaffolds made from bovine atelocollagen were fabricated. The scaffold structure mimicked the collagen arrangement in the osseous zone of osteochondral tissue (lamellar structure). Further investigations are required to compare lamellar spacing and pore size with cartilage characteristics. The characterization techniques of FTIR, XRD, SEM, EDS, and TGA further supported the claim of hydroxyapatite deposition formation within the scaffolds. Providing a possible solution to, indicating the mineralized collagen scaffold can be a promising candidate for subchondral bone defects repair.

Chapter 4 - Fabrication of Multizonal Scaffold

4.1. Introduction

Osteochondral tissue engineering seeks to restore the native articular cartilage and bone structural and functional characteristics. The development of scaffolds that can replicate the intricate structure of the natural osteochondral tissue is one of the field's biggest challenges. Multizonal scaffolds, which have several zones or areas that mimic the various characteristics of the cartilage and bone tissue, are being created to solve this issue. These scaffolds replicate each zone of the osteochondral tissue by being made of various materials and/or possessing various mechanical and/or biological qualities.

With collagen-based layers, these zones can be differentiated by directional freezing which controls pore size, homogeneity, and orientation (Arora et al., 2015). In addition, collagen creates the presence of a natural binding site and the ability to degrade overtime without the release of harmful products (Levingstone et al., 2014). As shown Figure 4.1, different zones can be directionally frozen to resemble the orientation of collagen fibers in different zones of osteochondral tissue. The transition zone oftentimes bonds both the vertical lamellar osseous zone and horizontal lamellar superficial zone. A multizonal scaffold mimicking the orientation of osteochondral tissue is then created via lyophilization, see Figure 4.1.

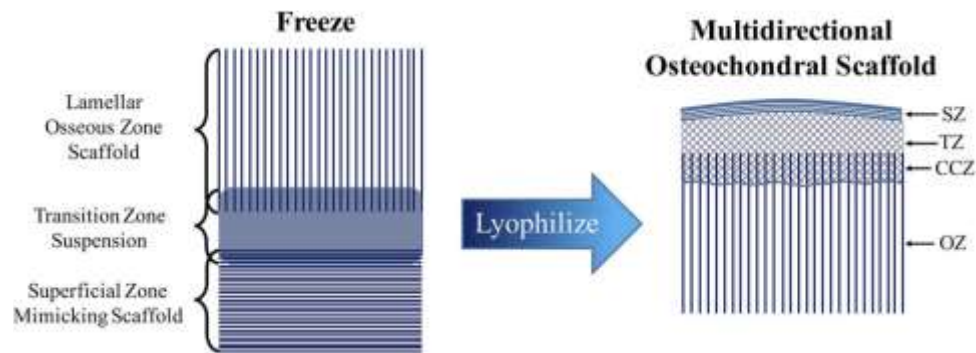


Figure 4.1. Illustration of directional freezing of scaffolds zones. Following with lyophilization to mimic the zones of osteochondral tissue: Superficial zone (SZ), transition zone (TZ), calcified cartilage zone (CCZ), and osseous zone (OZ) (Clearfield et al., 2018).

4.1.1. Fabrication

4.1.1.1. Lamella layers

The lamella layers are produced by collagen being unidirectionally frozen and growth of dendritic ice. The layer properties can be controlled based on the freezing conditions and the self-compression time of the gel. Base on the report by Xia et al., an increase in self-compression time led to a decrease in lamellar layer spacing (Xia et al., 2014). In addition, the wall thickness of the lamella layers increased. Another variable was the freezing temperature. It was found that a decrease in freezing temperature led to a decrease in lamellar spacing (Xia et al., 2014).

4.1.1.2. Freezing method

Various freezing methods can be conducted to control the orientation of the scaffold. To fabricate superficial and deep zones, unidirectional freezing is obtained by using insulation layers to properly guide ice growth. Unidirectional freezing involves

freezing in one direction that promotes pore alignment along that direction (Arora et al., 2015). In homogenous freezing, molds made from high thermal conductivity materials, such as metals, are used to allow freezing from all directions. This causes the pores and the structure of the scaffold to be non-directional. The purpose of the random freezing replicate the cellular structure of the middle zone in osteochondral tissue.

4.1.1.3. Lamellar osseous zone scaffold

The lamellar osseous zone is to mimic the subchondral bone and calcified cartilage layer of cartilage. It can be fabricated by radial freeze casting collagen-hydroxyapatite-containing suspension (Longley et al., 2018). A study on collagen-hydroxyapatite scaffolds for bone regeneration, co-precipitated type I collagen and hydroxyapatite (HA) in a modified simulated body fluid (Yu et al., 2020). The scaffold was then self-compressed and radially froze into a composite gel. The combination of radial freezing and self-compression processes created a multilevel lamellar structure of collagen. The lamellar osseous zone scaffold was then crosslinked to further enhance the mechanical properties. Factors, such as freezing temperature, freezing rate, and self-compression time, can influence the behavior of the pore size, porosity, and lamellae thickness (Xia et al., 2014). The lamellar structure of the mineralized collagen scaffold well mimics the structure and composition of the osseous zone of osteochondral tissue. This zone upholds the largest compressive forces acting on the scaffold as demonstrated in a study on pore orientation and mechanical behavior of collagen scaffolds by Arora et. al, shown in Figure 4.2 (Arora et al., 2015).

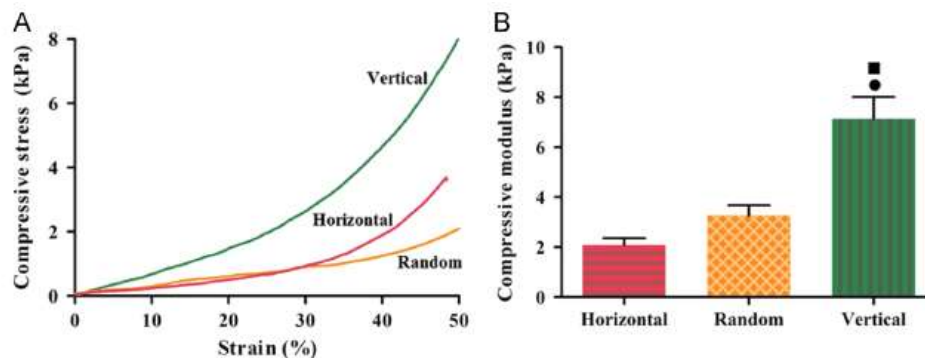


Figure 4.2. (a) Comparison of compressive stress vs strain between varying directions of pores. (b) Comparison of compressive moduli between varying directions of pores. (Arora et al., 2015).

4.1.1.4. Superficial zone scaffold

The superficial zone scaffold is fabricated to mimic the characterization of the superficial layer of the articular cartilage. A collagen-hyaluronic suspension was chosen to prepare this region to mimic the composition of the superficial zone in cartilage. The porous structure alignment was chosen to be horizontally or perpendicular to the force acting on the scaffold, in order to optimize the mechanical compressive properties. The least resistance and the lowest modulus at the lowest strain (Arora et al., 2015) are an ideal combination to support the stresses occurring at the joint. Hyaluronic acid (HyA) was chosen due to its abundance and biocompatibility within native cartilage, in addition to having an ideal degradation rate (Burdick et al., 2005). It has shown signs to promote chondrogenesis of MSCs by interactions with the CD44 and RHAMM cell receptors (Chen et al., 2015; Matsiko et al., 2012; Tang et al., 2007).

4.1.1.5. Transition zone scaffold

The adjoining site of the superficial and deep zones of the scaffold would be known as the transition zone. This zone must properly mimic the homogenous structure of the transition zone of articular cartilage by creating an equiaxed structure (Xia et al., 2014). This zone is oftentimes prone to separation or tearing based on previous work on fabricating such multilayered scaffolds (Jia et al., 2018; Li et al., 2015). Approaches of BioGlue, a synthetic tidemark, or varying quantity of mineralization throughout each layer have been attempted to address the issue (Hu et al., 2022; Kandel, 1999; Kesireddy & Kasper, 2016), but limitations in cell proliferation, tissue regeneration, and biodegradation were observed (Yu et al., 2023).

4.2. Methods and Materials

Three approaches were attempted to prepare multizonal scaffolds, as listed in Table 4.1. Each of the approaches involved the use of a combination of collagen lamellar hydroxyapatite scaffold and a collagen-hyaluronic acid suspension. Lyophilization was also utilized in all attempts to form cartilage-mimicking multizonal scaffolds.

Lyophilization of the middle and superficial layers onto the osseous layer was optimized. This process began with the fabrication of the collagen-lamellar hydroxyapatite scaffold as described in Chapter 3. This scaffold was then cut using a sterilized razor blade, into a rectangular prism that was dimensioned approximately 6 X 6 X 11 mm. A polymethyl methacrylate (PMMA) mold was designed with the following criteria: a 7 X 7 X 29 mm through hole (lubricated with vegetable oil), with a 5.5 mm PMMA wall thickness. An additional extension from the halfway point of the through hole was created to make a T shape design. This additional extension was approximately 11 mm. Copper

plates were secured on each end to ensure liquid tight sealing and proper freezing direction. Components of this mold were adapted from our previous study (Clearfield et. al, 2017). The T-shaped mold was designed to promote organized directional freezing, as shown in Figure 4.3.

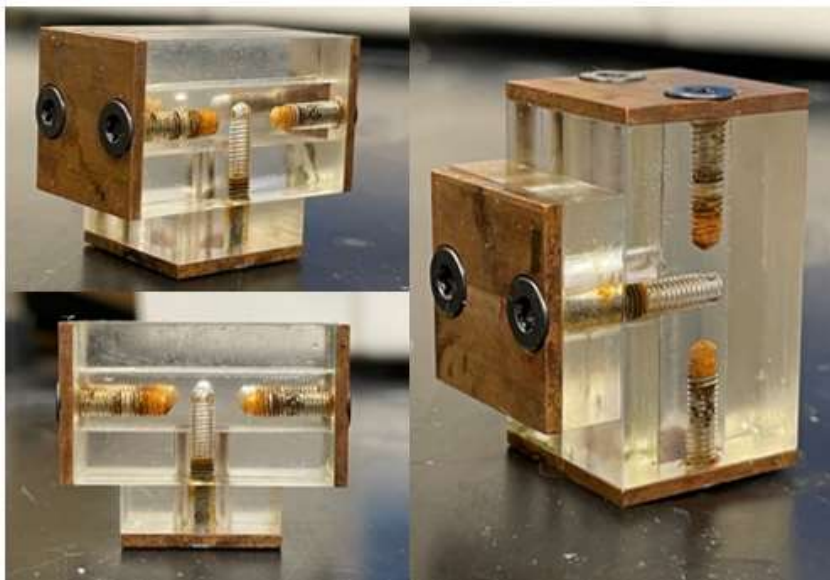


Figure 4.3. T-shaped PMMA mold used for directional freezing.

The chondral mimicking zones were fabricated using type I collagen and hyaluronic acid suspension. Collagen from Chapter 2 was isolated and freeze dried. The pepsin-soluble collagen and hyaluronic acid (SIGMA-ALDRICH; 53747-1G) were mixed at a 9:1 (w/w) ratio. Which were then added to a 0.5 M acetic acid solution at a 1:50 (w/v) ratio. The entire suspension was homogenized over ice using a rotar-stator homogenizer (OMNI International; TH-01) for 1 hour. The suspension was then degassed by centrifuging (Thermo Scientific Sorvall Legend XT/XF series ; 75004521) at 1500 RPMs for 15 minutes. Approximately 3 mL of the collagen-hyaluronic acid suspension was then loaded into the top of T-shaped PMMA mold with copper plates on each end. The suspension was

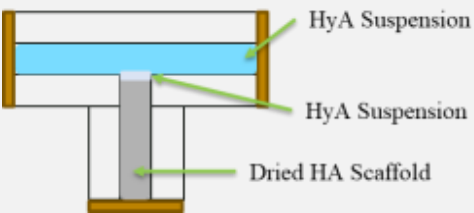
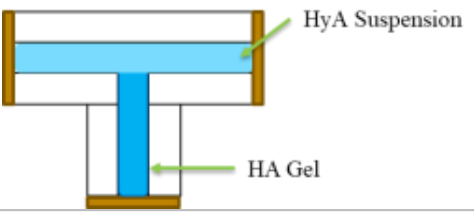
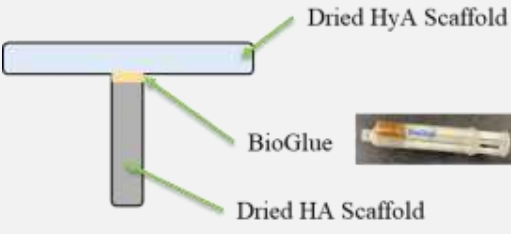
then placed in the Labconco Corporation freeze dryer and tray dryer combo at -40°C , for 12 hours. Following the freezing, 1 mL of the collagen-hyaluronic acid suspension was loaded into the mold's extension followed by the collagen lamellar-hydroxyapatite scaffold, shown in Table 4.1.a. The mold was then sealed shut by copper plates and placed in the freeze dryer at -40°C , for at least 24 hours, to freeze the entire scaffold. Following the freezing, one of the copper plates were removed and a vacuum (0.010 mbar) was initiated for 72 hours.

Variations of this protocol were also conducted. The collagen-hyaluronic acid suspension (9:1) (w/w) was used in conjunction with the hydroxyapatite collagen solution, as stated in Chapter 3, at its gelled state. After the hydroxyapatite collagen solution had undergone the 12-hour at 37°C water bath inside of the PMMA mold, the collagen-hyaluronic acid suspension was then loaded into mold as seen in Table 4.1.b. The mold was then sealed shut by copper plates and placed in the freeze dryer at -40°C , for at least 24 hours, to freeze the entire scaffold. Following the freezing, one of the copper plates were removed and a vacuum (0.010 mbar) was initiated for 72 hours.

The last fabrication method involved unidirectional collagen-hyaluronic acid scaffold and collagen lamellar-hydroxyapatite scaffold. Each of these scaffolds were dried and cut accordingly; collagen-hyaluronic acid scaffold – 6 X 6 X 25 mm and collagen lamellar-hydroxyapatite scaffold – 6 X 6 X 11 mm. Bioglue® (CryoLife; BG3515-5-US) was then placed atop of the collagen lamellar-hydroxyapatite scaffold and pressed into the midway point of the collagen-hyaluronic acid scaffold. The Bioglue was left to dry for 1-hour. This composition can be seen in Table 4.1.c.

The multizonal scaffolds were then crosslinked using MES monohydrate buffer, EDC, and NHS with DIW. The solution was then titrated to pH=5 using drop wise addition of HCl. The multizonal scaffold was then placed in the solution for 4 hours after pressing it with a disinfected spatula to ensure all air bubbles were evacuated from the inner pores. After 4 hours, the scaffold was immersed in 5% glycine to DIW (w/v) for 12 hours. After sitting in 5% glycine, the scaffold was rinsed thrice, freeze dried and stored at 4° C.

Table 4.1. Multizonal scaffold fabrication methods and their respective compositions.

Multizonal fabrication method	Scaffold Composition
<p>a.</p> 	<p>Collagen and hyaluronic acid 9:1 (w/w) suspension and collagen lamellar-hydroxyapatite scaffold.</p>
<p>b.</p> 	<p>Collagen and hyaluronic acid 9:1 (w/w) suspension and hydroxyapatite collagen gel.</p>
<p>c.</p> 	<p>Collagen and hyaluronic acid 9:1 (w/w) scaffold, collagen lamellar-hydroxyapatite scaffold, and BioGlue.</p>

4.2.1. Scaffold Characterization

4.2.1.1. SEM

The cross sections of the multizonal scaffold were observed using scanning electron microscopy (SEM; JEOL JSM-639OLV). Magnification images of x60 were captured for each zone of the scaffold, including superficial zone, transition zone, and osseous zone. These images were then stitched together using MosaicJ plugin through the ImageJ software.

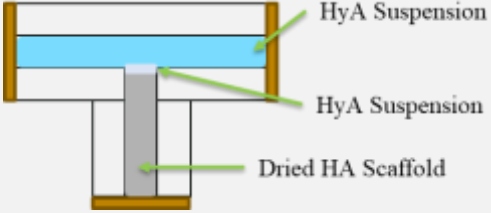
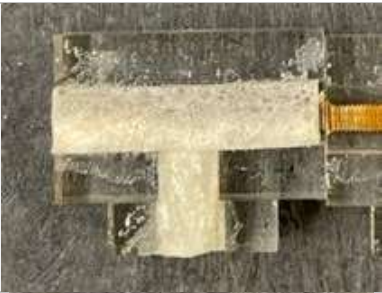
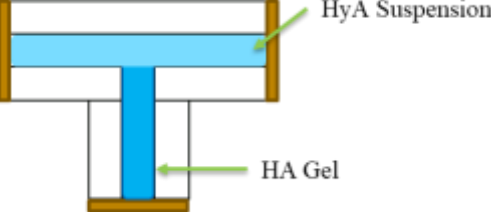
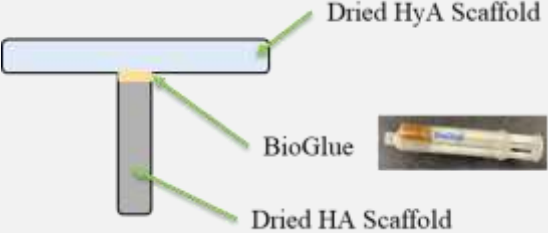
4.2.1.2. FTIR

The surface functional groups of the collagen-hyaluronic acid and collagen-lamellar mineralized scaffolds were characterized using Fourier transform infrared spectroscopy (FTIR; Perkin Elmer Spectrum 65 FT-IR) with an attenuated total reflection unit (ATR; SensIR Technologies, 071-1514) over a range of 4000–500 cm^{-1} .

4.3. Results

The visual results of multizonal scaffold formed with their respective method are shown in Table 4.2. The collagen-hyaluronic acid suspension and dried collagen-hydroxyapatite scaffold showed the best results by first glance, seen in Table 4.2.a. Due to the success of the method 4.2.a, this was further analyzed for characterization. The 4.2.b method showed scaffold integration to be fragile and instable once removed from the mold. The 4.2.c method also showed instability at the bonding interface.

Table 4.2. Visual results of each multizonal method. (a) HyA suspension + dried HA scaffold. (b) HyA suspension + HA gel. (c) HyA scaffold + HA scaffold bonded by BioGlue.

Multizonal Method	Visual Results
<p>a.</p> 	
<p>b.</p> 	
<p>c.</p> 	

4.3.1. Characterization results

4.3.1.1. SEM

The multizonal scaffold cross-section was observed using scanning electron microscopy (SEM) at a magnification of x60, as shown in Figure 4.4. A clear horizontal lamellar structure was observed in the superficial zone, while a vertical lamellar structure is present in the osseous zone. Each lamella is composed of multiple mini-lamellae. The interlamellar distance of two adjacent lamellae in the superficial zone was measured using

the ImageJ software of the 2D images. It was found that the average distance was $62.7 \pm 12.11 \mu\text{m}$ of the superficial zone. The transition zone demonstrates a cellular structure mimicking the transition zone of osteochondral tissue. The average pore size of the cellular structure was found to be $83.7 \pm 16.32 \mu\text{m}$. The average interlamellar distance of the osseous zone was found to be $166.4 \pm 77.33 \mu\text{m}$.

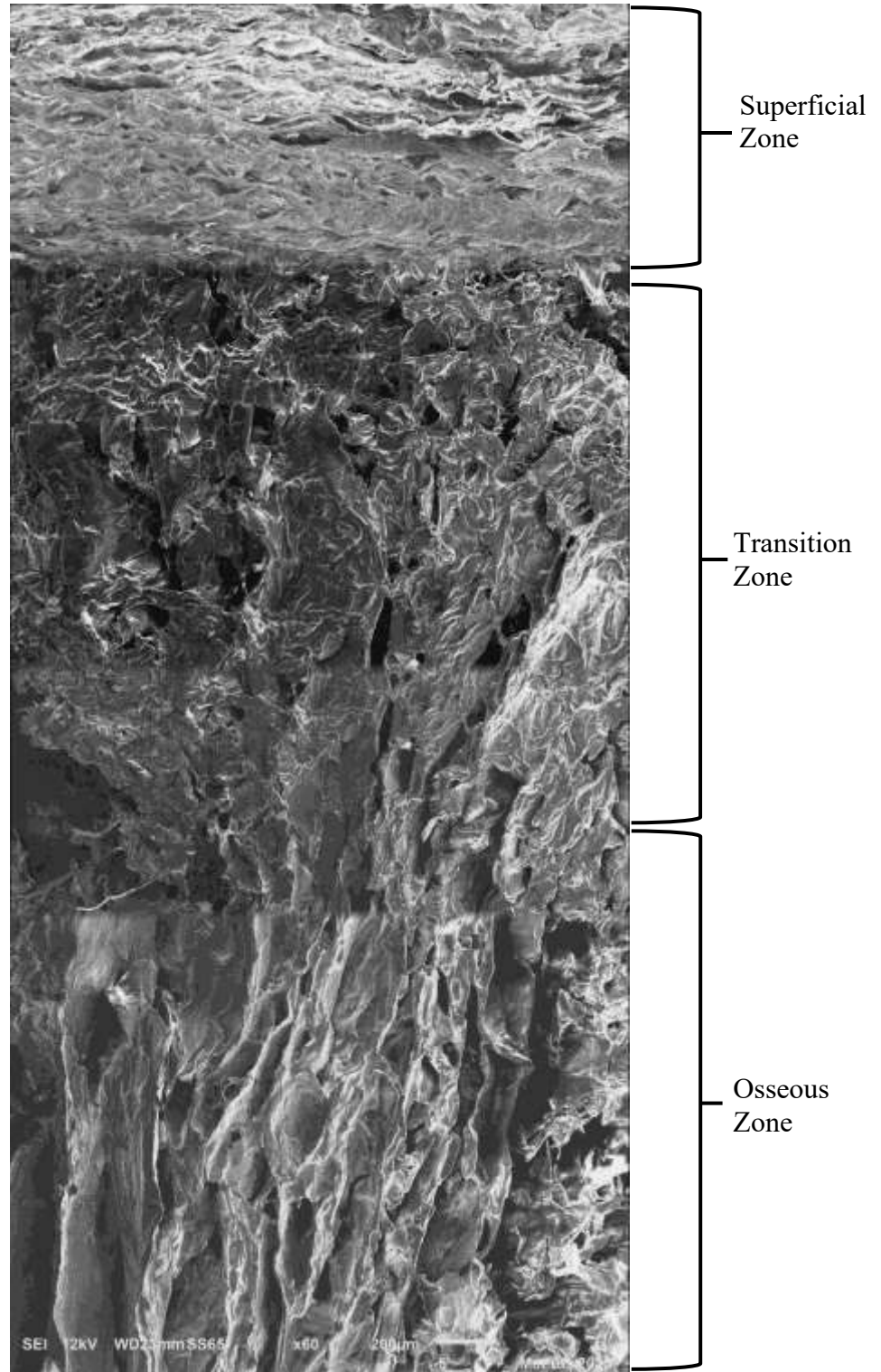


Figure 4.4. Combined SEM image of osseous zone (bottom) to superficial zone (top) of multizonal scaffold at x60 magnification.

4.3.1.2. FTIR

The FTIR spectra was analyzed for the collagen-hyaluronic acid scaffold and collagen-hydroxyapatite lamellar scaffold. The notable peaks for each scaffold were labeled according to our previous study (Clearfield et al., 2018). The amide I, II, and III bands are reflected from collagen. Followed by the C-O stretching occurring at approximately 1000 cm^{-1} .

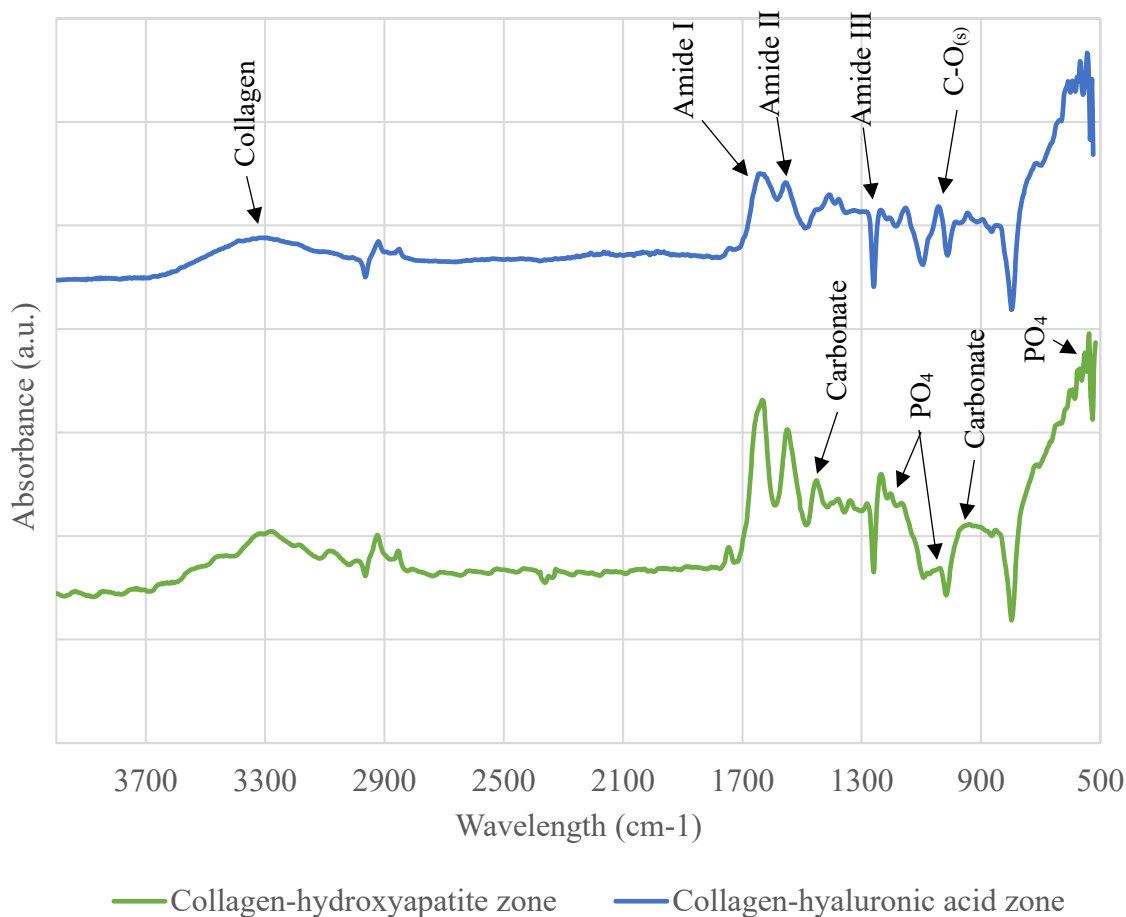


Figure 4.5. FTIR of collagen-hydroxyapatite lamellar zone and collagen-hyaluronic acid zone of a multizonal scaffold.

4.4. Discussion

Restoring native osteochondral tissue is an area investigated by many research groups across the globe (Levingstone et al., 2016; Parisi et al., 2020; Zhou et al., 2020). Despite of all these efforts, successfully mimicking the zonal architectural structure and function has yet to be achieved. Without the use of a biocompatible solution, the patient's body will often reject the proliferation of native chondrocytes and osteocytes, leading to a lack of tissue regeneration and poor mechanical properties.

This study took three routes in sight of satisfying these conditions. Each of the solutions involved a collagen-hyaluronic acid zone that replicates the chondral sections of articular cartilage. Followed by a mineralized collagen suspension replicating the osseous section of subchondral bone. The first approach, as shown in Table 4.2.a, produced the optimal results of the three. The collagen-hyaluronic acid suspension was lyophilized onto the dried collagen hydroxyapatite lamellar scaffold, resulting in a well-integrated structure that supported the collagen alignment of native cartilage tissue. Starting from deep, the lamellar osseous structure mimicked the vertical collagen alignment of the osseous and deep zones of osteochondral tissue (Sophia Fox et al., 2009). With directional freezing, a clear lamellar structure was formed which was used to serve as superficial and osseous zones of the multizonal scaffold, shown in Figure 4.6.a. In contrast, with homogenous freezing, a cellular structure was achieved by random ice growth resulting in an equiaxed structure, shown in Figure 4.6.b (Xia et al., 2013), which served as the transition zone in the multizonal scaffold. The success of the integration of each layer is shown in the SEM image of Figure 4.4.

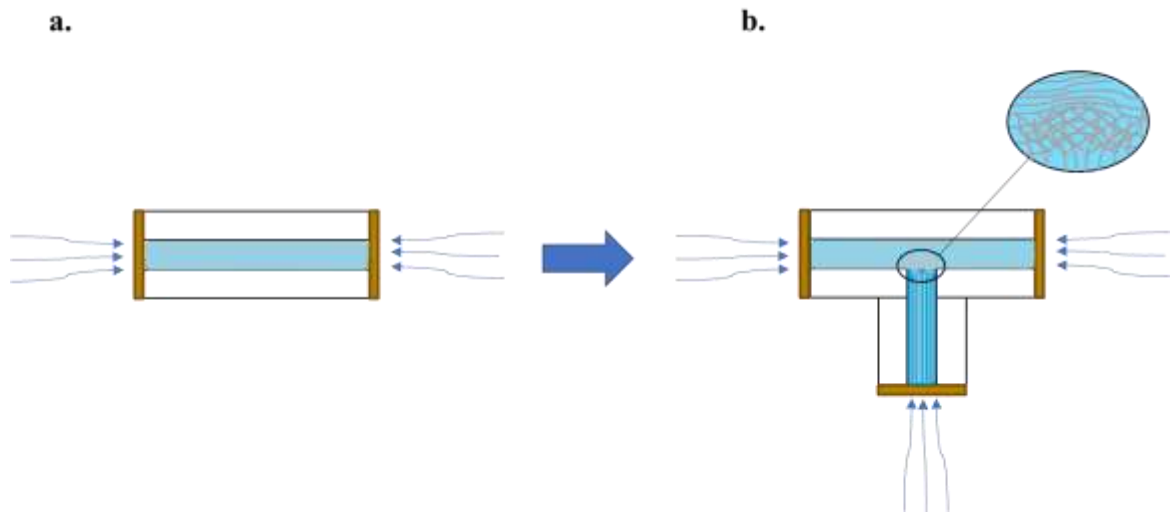


Figure 4.6. (a) Unidirectional freezing resulting in the superficial zone. (b) Homogenous freezing resulting in transition zone of a cellular structure.

In the second approach (Table 4.1.b), lyphollization of a collagen-hyaluronic acid suspension and collagen hydroxyapatite gel was considered due to possible enhanced layer integration. After SEM analysis of the scaffold, there was shown to be a clear debonding between two zones. The transition zone did not properly form, which resulted in weak bonding between the layers, shown in Figure 4.7.

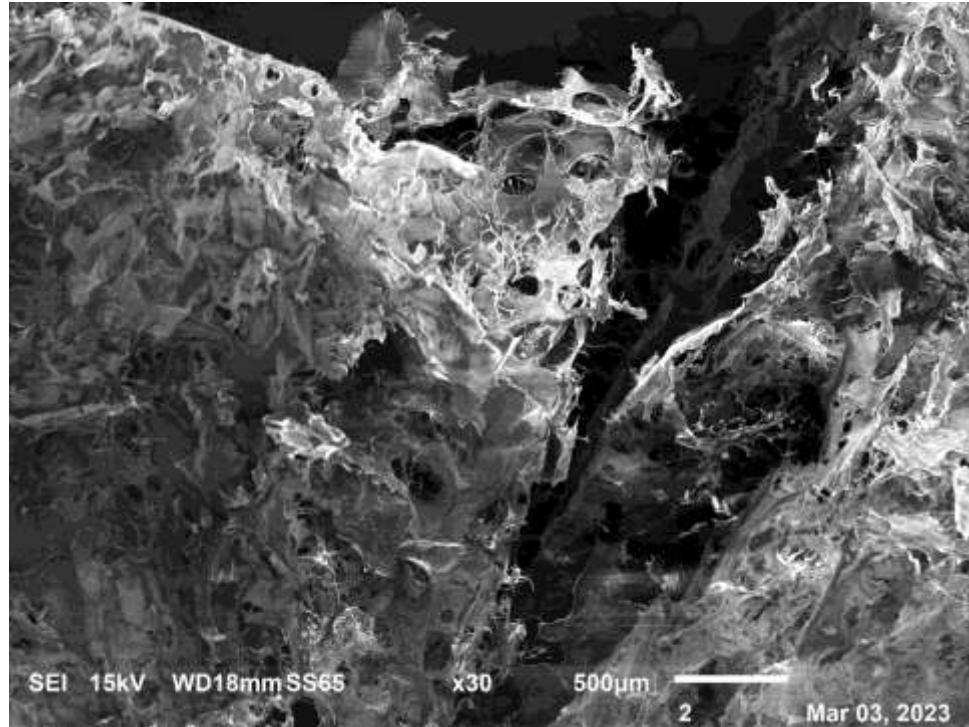


Figure 4.7. SEM image of collagen HyA scaffold and collagen HA scaffold with separation between layers for the second approach.

It was also noticed that due to the hydrogel state, once the scaffold was freeze dried, the mineralized section shrank significantly due to removal of ice molecules, creating a gap at the interface between the superficial and osseous zones (Xu et al., 2021).

The third approach involving the use of BioGlue to bond two dried scaffolds of superficial and deep zones, as shown in Table 4.2.c. It was found that generally the bonding between the zones of the multizonal scaffold are enhanced, but the low permeability of BioGlue restricts cell migration and differentiation (Yu et al., 2023). This could lead to poor integration between multizonal scaffolds and surrounding native tissue (Dormer et al., 2010). Figure 4.8 shows an SEM image of the BioGlue, which demonstrates a dense structure with poor bonding to the surrounding scaffold.

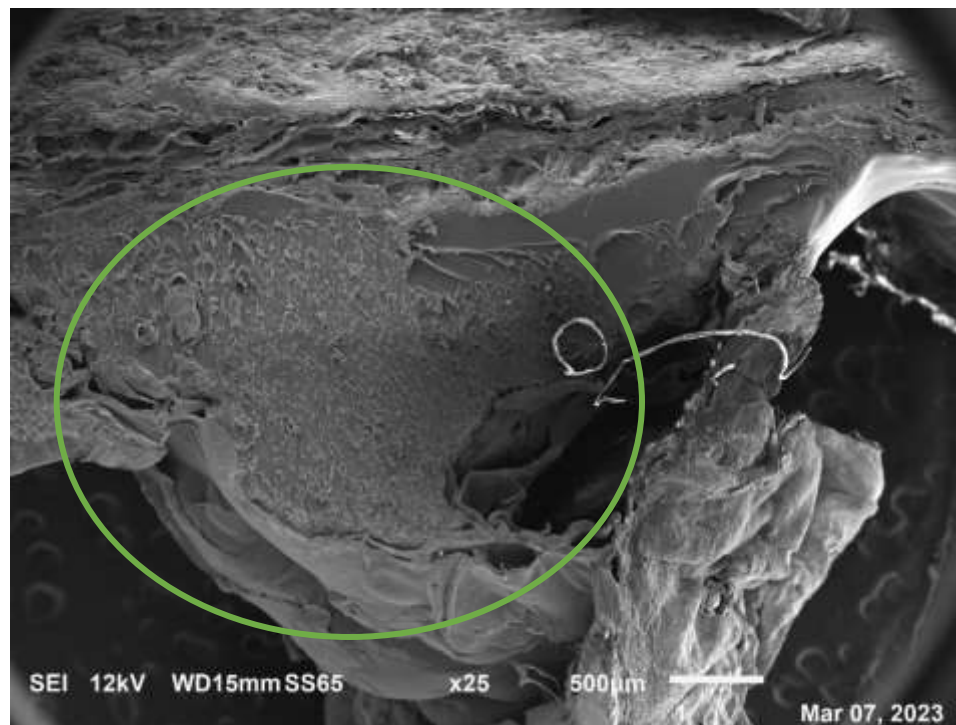


Figure 4.8. SEM image of BioGlue used to integrate each scaffold. The circle area is the BioGlue, which has demonstrates a dense structure.

4.5. Conclusions

In Chapter 4, a multizonal scaffold with composition and structure closely mimicking those of osteochondral tissue has been successfully fabricated. The use of a mix of hyaluronic-acid and collagen and mineralized collagen as respective superficial and deep zones of the multizonal scaffold closely mimic the composition of osteochondral tissue. Freezing parameters were optimized to imitate each zone of cartilage. Lyophilization of the zones to incorporate structural integration was utilized. The engineering of multizonal scaffolds with structure and composition mimicking the nature tissue holds great promises for osteochondral tissue repair and regeneration.

Chapter 5 - Summary/Future Directions

This study has successfully developed a novel collagen-based, multizonal scaffold for osteochondral repair applications. The present study involved the extraction of collagen from bovine tendon achilles. Atelocollagen was derived and used to fabricate multizonal collagen-based scaffolds. Each zone of the scaffold mimicked a particular zone of osteochondral tissue. Fabrication of collagen scaffolds that mimic the specific orientation of each layer of articular cartilage (middle, deep, and calcified cartilage/subchondral bone zones) was shown to be successful. This was conducted by lyophilization of a collagen-hyaluronic acid suspension and a collagen hydroxyapatite scaffold. Structural arrangement of the zones was controlled by directional freezing in order to reproduce the lamellae orientation of native articular cartilage tissue. Characterization of SEM, EDS, XRD, FTIR, and TGA further verified the deposition of hydroxyapatite in the deep zone and proper lamellae within the scaffold. Studies involving biodegradability study, mechanical testing, and *in vitro* and *in vivo* experimentation would need to be further investigated before clinical use.

Chapter 6 - References

- Abou Neel, E. A., Bozec, L., Knowles, J. C., Syed, O., Mudera, V., Day, R., & Hyun, J. K. (2013). Collagen--emerging collagen based therapies hit the patient. *Adv Drug Deliv Rev*, 65(4), 429-456. <https://doi.org/10.1016/j.addr.2012.08.010>
- Ahn, J.-I., Kuffova, L., Merrett, K., Mitra, D., Forrester, J. V., Li, F., & Griffith, M. (2013). Crosslinked collagen hydrogels as corneal implants: Effects of sterically bulky vs. non-bulky carbodiimides as crosslinkers. *Acta Biomaterialia*, 9(8), 7796-7805. <https://doi.org/https://doi.org/10.1016/j.actbio.2013.04.014>
- Al-Munajjed, A. A., Plunkett, N. A., Gleeson, J. P., Weber, T., Jungreuthmayer, C., Levingstone, T., Hammer, J., & O'Brien, F. J. (2009). Development of a biomimetic collagen-hydroxyapatite scaffold for bone tissue engineering using a SBF immersion technique. *Journal of Biomedical Materials Research Part B: Applied Biomaterials*, 90B(2), 584-591. <https://doi.org/https://doi.org/10.1002/jbm.b.31320>
- Arora, A., Kothari, A., & Katti, D. S. (2015). Pore orientation mediated control of mechanical behavior of scaffolds and its application in cartilage-mimetic scaffold design. *J Mech Behav Biomed Mater*, 51, 169-183. <https://doi.org/10.1016/j.jmbbm.2015.06.033>
- Aukkanit, N., & Garnjanagoonchorn, W. (2010). Temperature effects on type I pepsin-solubilised collagen extraction from silver-line grunt skin and its in vitro fibril self-assembly [Article]. *Journal of the Science of Food and Agriculture*, 90(15), 2627-2632. <https://doi.org/10.1002/jsfa.4131>
- Baumann, C., Hinckel, B., Bozynski, C., & Farr, J. (2019). Articular Cartilage: Structure and Restoration: A Clinical Casebook. In (pp. 3-24). https://doi.org/10.1007/978-3-030-01491-9_1
- Bhosale, A. M., & Richardson, J. B. (2008). Articular cartilage: structure, injuries and review of management. *British Medical Bulletin*, 87(1), 77-95. <https://doi.org/10.1093/bmb/ldn025>
- Boskey, A. (2007). Mineralization of Bones and Teeth. *Elements*, 3, 385-391. <https://doi.org/10.2113/GSELEMENTS.3.6.385>
- Boskey, A. L., & Robey, P. G. (2013). The Composition of Bone. In *Primer on the Metabolic Bone Diseases and Disorders of Mineral Metabolism* (pp. 49-58). <https://doi.org/https://doi.org/10.1002/9781118453926.ch6>
- Buckwalter, J. A., & Mankin, H. J. (1998). Articular cartilage repair and transplantation. *Arthritis Rheum*, 41(8), 1331-1342. [https://doi.org/10.1002/1529-0131\(199808\)41:8<1331::Aid-art2>3.0.Co;2-j](https://doi.org/10.1002/1529-0131(199808)41:8<1331::Aid-art2>3.0.Co;2-j)
- Burdick, J. A., Chung, C., Jia, X., Randolph, M. A., & Langer, R. (2005). Controlled degradation and mechanical behavior of photopolymerized hyaluronic acid networks. *Biomacromolecules*, 6(1), 386-391. <https://doi.org/10.1021/bm049508a>
- Cavelier, S., Yu, L., Hannon, B., & Wei, M. (2023). In Progress: Fabrication and Development of Multizonal Scaffolds for Osteochondral Repair.

- Chen, F. H., Rousche, K. T., & Tuan, R. S. (2006). Technology Insight: adult stem cells in cartilage regeneration and tissue engineering. *Nature Clinical Practice Rheumatology*, 2(7), 373-382. <https://doi.org/10.1038/ncprheum0216>
- Chen, S., Zhang, Q., Kawazoe, N., & Chen, G. (2015). Effect of high molecular weight hyaluronic acid on chondrocytes cultured in collagen/hyaluronic acid porous scaffolds [10.1039/C5RA18755A]. *RSC Advances*, 5(114), 94405-94410. <https://doi.org/10.1039/C5RA18755A>
- Christiansen, D. L., Huang, E. K., & Silver, F. H. (2000). Assembly of type I collagen: Fusion of fibril subunits and the influence of fibril diameter on mechanical properties [Article]. *Matrix Biology*, 19(5), 409-420. [https://doi.org/10.1016/S0945-053X\(00\)00089-5](https://doi.org/10.1016/S0945-053X(00)00089-5)
- Clearfield, D., Nguyen, A., & Wei, M. (2018). Biomimetic multidirectional scaffolds for zonal osteochondral tissue engineering via a lyophilization bonding approach. *J Biomed Mater Res A*, 106(4), 948-958. <https://doi.org/10.1002/jbm.a.36288>
- Deng, C., Xu, C., Zhou, Q., & Cheng, Y. (2019). Advances of nanotechnology in osteochondral regeneration. *Wiley Interdiscip Rev Nanomed Nanobiotechnol*, 11(6), e1576. <https://doi.org/10.1002/wnan.1576>
- Dey, S., & Pal, S. (2009, 2009//). Evaluation of Collagen-hydroxyapatite Scaffold for Bone Tissue Engineering. 13th International Conference on Biomedical Engineering, Berlin, Heidelberg.
- Deymier, A. C., An, Y., Boyle, J. J., Schwartz, A. G., Birman, V., Genin, G. M., Thomopoulos, S., & Barber, A. H. (2017). Micro-mechanical properties of the tendon-to-bone attachment. *Acta Biomater*, 56, 25-35. <https://doi.org/10.1016/j.actbio.2017.01.037>
- Dormer, N. H., Berkland, C. J., & Detamore, M. S. (2010). Emerging Techniques in Stratified Designs and Continuous Gradients for Tissue Engineering of Interfaces. *Annals of Biomedical Engineering*, 38(6), 2121-2141. <https://doi.org/10.1007/s10439-010-0033-3>
- Ellingson, A. J., Pancheri, N. M., & Schiele, N. R. (2022). Regulators of collagen crosslinking in developing and adult tendons. *Eur Cell Mater*, 43, 130-152. <https://doi.org/10.22203/eCM.v043a11>
- Filip Ionescu, O. L., Mocanu, A. G., Neacșu, I. A., Ciocîlteu, M. V., Rău, G., & Neamțu, J. (2022). Biocompatibility Studies on a Collagen-Hydroxyapatite Biomaterial. *Curr Health Sci J*, 48(2), 217-225. <https://doi.org/10.12865/chsj.48.02.12>
- Fratzl, P. (2003). Cellulose and collagen: From fibres to tissues [Review]. *Current Opinion in Colloid and Interface Science*, 8(1), 32-39. [https://doi.org/10.1016/S1359-0294\(03\)00011-6](https://doi.org/10.1016/S1359-0294(03)00011-6)
- Fratzl, P. (2008). Collagen: Structure and mechanics, an introduction. In *Collagen: Structure and Mechanics* (pp. 1-13). https://doi.org/10.1007/978-0-387-73906-9_1
- Friess, W. (1998). Collagen - Biomaterial for drug delivery [Article]. *European Journal of Pharmaceutics and Biopharmaceutics*, 45(2), 113-136. [https://doi.org/10.1016/S0939-6411\(98\)00017-4](https://doi.org/10.1016/S0939-6411(98)00017-4)

- Gross, A. E., Kim, W., Las Heras, F., Backstein, D., Safir, O., & Pritzker, K. P. (2008). Fresh osteochondral allografts for posttraumatic knee defects: long-term followup. *Clin Orthop Relat Res*, 466(8), 1863-1870. <https://doi.org/10.1007/s11999-008-0282-8>
- Holmes, R., Kirk, S., Tronci, G., Yang, X., & Wood, D. (2017). Influence of telopeptides on the structural and physical properties of polymeric and monomeric acid-soluble type I collagen. *Mater Sci Eng C Mater Biol Appl*, 77, 823-827. <https://doi.org/10.1016/j.msec.2017.03.267>
- Hong, H., Chaplot, S., Chalamaiah, M., Roy, B. C., Bruce, H. L., & Wu, J. (2017). Removing Cross-Linked Telopeptides Enhances the Production of Low-Molecular-Weight Collagen Peptides from Spent Hens. *Journal of Agricultural and Food Chemistry*, 65(34), 7491-7499. <https://doi.org/10.1021/acs.jafc.7b02319>
- Hoshi, K., Fujihara, Y., Asawa, Y., Nishizawa, S., Kanazawa, S., Sakamoto, T., Watanabe, M., Ogasawara, T., Saijo, H., Mori, Y., & Takato, T. (2013). Recent trends in cartilage regenerative medicine and its application to oral and maxillofacial surgery [Review]. *Oral Science International*, 10(1), 15-19. [https://doi.org/10.1016/S1348-8643\(12\)00049-3](https://doi.org/10.1016/S1348-8643(12)00049-3)
- Hu, X., Zheng, S., Zhang, R., Wang, Y., Jiao, Z., Li, W., Nie, Y., Liu, T., & Song, K. (2022). Dynamic process enhancement on chitosan/gelatin/nano-hydroxyapatite-bone derived multilayer scaffold for osteochondral tissue repair. *Biomaterials Advances*, 133, 112662. <https://doi.org/https://doi.org/10.1016/j.msec.2022.112662>
- Huber, M., Trattinig, S., & Lintner, F. (2000). Anatomy, biochemistry, and physiology of articular cartilage. *Invest Radiol*, 35(10), 573-580. <https://doi.org/10.1097/00004424-200010000-00003>
- Jia, S., Wang, J., Zhang, T., Pan, W., Li, Z., He, X., Yang, C., Wu, Q., Sun, W., Xiong, Z., & Hao, D. (2018). Multilayered Scaffold with a Compact Interfacial Layer Enhances Osteochondral Defect Repair. *ACS Applied Materials & Interfaces*, 10(24), 20296-20305. <https://doi.org/10.1021/acsami.8b03445>
- Jiang, S., Guo, W., Tian, G., Luo, X., Peng, L., Liu, S., Sui, X., Guo, Q., & Li, X. (2020). Clinical Application Status of Articular Cartilage Regeneration Techniques: Tissue-Engineered Cartilage Brings New Hope. *Stem cells international*, 2020, 5690252-5690252. <https://doi.org/10.1155/2020/5690252>
- Ju, H., Liu, X., Zhang, G., Liu, D., & Yang, Y. (2020). Comparison of the Structural Characteristics of Native Collagen Fibrils Derived from Bovine Tendons using Two Different Methods: Modified Acid-Solubilized and Pepsin-Aided Extraction. *Materials (Basel, Switzerland)*, 13(2), 358. <https://doi.org/10.3390/ma13020358>
- Kaku, M., Rosales Rocabado, J. M., Kitami, M., Ida, T., Akiba, Y., Yamauchi, M., & Uoshima, K. (2016). Mechanical Loading Stimulates Expression of Collagen Cross-Linking Associated Enzymes in Periodontal Ligament. *J Cell Physiol*, 231(4), 926-933. <https://doi.org/10.1002/jcp.25184>
- Kandel, R. M. H., and Marc Grynepas. (1999). Characterization of the Mineral in Calcified Articular Cartilagenous Tissue Formed in Vitro. *Tissue Engineering*, 5(1), 25-34. <https://doi.org/10.1089/ten.1999.5.25>

- Kesireddy, V., & Kasper, F. K. (2016). Approaches for building bioactive elements into synthetic scaffolds for bone tissue engineering [10.1039/C6TB00783J]. *Journal of Materials Chemistry B*, 4(42), 6773-6786. <https://doi.org/10.1039/C6TB00783J>
- Ketnawa, S., Benjakul, S., Martínez-Alvarez, O., & Rawdkuen, S. (2017). Fish skin gelatin hydrolysates produced by visceral peptidase and bovine trypsin: Bioactivity and stability. *Food Chemistry*, 215, 383-390. <https://doi.org/https://doi.org/10.1016/j.foodchem.2016.07.145>
- Khong, N. M. H., Yusoff, F. M., Jamilah, B., Basri, M., Maznah, I., Chan, K. W., Armania, N., & Nishikawa, J. (2018). Improved collagen extraction from jellyfish (*Acromitus hardenbergi*) with increased physical-induced solubilization processes. *Food Chemistry*, 251, 41-50. <https://doi.org/https://doi.org/10.1016/j.foodchem.2017.12.083>
- Kilian, D., Ahlfeld, T., Akkineni, A. R., Bernhardt, A., Gelinsky, M., & Lode, A. (2020). 3D Bioprinting of osteochondral tissue substitutes – in vitro-chondrogenesis in multi-layered mineralized constructs. *Scientific Reports*, 10(1), 8277. <https://doi.org/10.1038/s41598-020-65050-9>
- Killen, M.-C., & Charalambous, C. P. (2020). Chapter 6 - Advances in cartilage restoration techniques. In W. Ahmed, D. A. Phoenix, M. J. Jackson, & C. P. Charalambous (Eds.), *Advances in Medical and Surgical Engineering* (pp. 71-83). Academic Press. <https://doi.org/https://doi.org/10.1016/B978-0-12-819712-7.00006-1>
- Knott, L., & Bailey, A. J. (1998). Collagen cross-links in mineralizing tissues: a review of their chemistry, function, and clinical relevance. *Bone*, 22(3), 181-187. [https://doi.org/10.1016/s8756-3282\(97\)00279-2](https://doi.org/10.1016/s8756-3282(97)00279-2)
- Kumar, A., Kargozar, S., Baino, F., & Han, S. S. (2019). Additive Manufacturing Methods for Producing Hydroxyapatite and Hydroxyapatite-Based Composite Scaffolds: A Review [Review]. *Frontiers in Materials*, 6. <https://doi.org/10.3389/fmats.2019.00313>
- Kuznetsova, N., & Leikin, S. (1999). Does the triple helical domain of type I collagen encode molecular recognition and fiber assembly while telopeptides serve as catalytic domains? Effect of proteolytic cleavage on fibrillogenesis and on collagen-collagen interaction in fibers. *J Biol Chem*, 274(51), 36083-36088. <https://doi.org/10.1074/jbc.274.51.36083>
- L'Heureux, N., Pâquet, S., Labbé, R., Germain, L., & Auger, F. A. (1998). A completely biological tissue-engineered human blood vessel. *Faseb j*, 12(1), 47-56. <https://doi.org/10.1096/fasebj.12.1.47>
- Lee, E. H., Chun, S. Y., Lee, J. N., Yoon, B. H., Chung, J. W., Han, M. H., Kwon, T. G., Ha, Y. S., & Kim, B. S. (2022). Optimized Collagen Extraction Process to Obtain High Purity and Large Quantity of Collagen from Human Perirenal Adipose Tissue. *Biomed Res Int*, 2022, 3628543. <https://doi.org/10.1155/2022/3628543>
- León-López, A., Morales-Peñaloza, A., Martínez-Juárez, V., Vargas-Torres, A., Zeugolis, D., & Aguirre-Álvarez, G. (2019). Hydrolyzed Collagen—Sources and Applications. *Molecules*, 24, 4031. <https://doi.org/10.3390/molecules24224031>

- Levingstone, T. J., Matsiko, A., Dickson, G. R., O'Brien, F. J., & Gleeson, J. P. (2014). A biomimetic multi-layered collagen-based scaffold for osteochondral repair [Article]. *Acta Biomaterialia*, *10*(5), 1996-2004.
<https://doi.org/10.1016/j.actbio.2014.01.005>
- Levingstone, T. J., Thompson, E., Matsiko, A., Schepens, A., Gleeson, J. P., & O'Brien, F. J. (2016). Multi-layered collagen-based scaffolds for osteochondral defect repair in rabbits. *Acta Biomater*, *32*, 149-160.
<https://doi.org/10.1016/j.actbio.2015.12.034>
- Li, J., Wang, M., Qiao, Y., Tian, Y., Liu, J., Qin, S., & Wu, W. (2018). Extraction and characterization of type I collagen from skin of tilapia (*Oreochromis niloticus*) and its potential application in biomedical scaffold material for tissue engineering [Article]. *Process Biochemistry*, *74*, 156-163.
<https://doi.org/10.1016/j.procbio.2018.07.009>
- Li, X., Ding, J., Wang, J., Zhuang, X., & Chen, X. (2015). Biomimetic biphasic scaffolds for osteochondral defect repair. *Regenerative biomaterials*, *2*(3), 221-228.
<https://doi.org/10.1093/rb/rbv015>
- Lin, K., Zhang, D., Macedo, M. H., Cui, W., Sarmiento, B., & Shen, G. (2019). Advanced Collagen-Based Biomaterials for Regenerative Biomedicine. *Advanced Functional Materials*, *29*(3), 1804943.
<https://doi.org/https://doi.org/10.1002/adfm.201804943>
- Liu, X. D., Skold, M., Umino, T., Zhu, Y. K., Romberger, D. J., Spurzem, J. R., & Rennard, S. I. (2000). Endothelial cell-mediated type I collagen gel contraction is regulated by hemin. *J Lab Clin Med*, *136*(2), 100-109.
<https://doi.org/10.1067/mlc.2000.108153>
- Longley, R., Ferreira, A. M., & Gentile, P. (2018). Recent approaches to the manufacturing of biomimetic multi-phasic scaffolds for osteochondral regeneration [Review]. *International Journal of Molecular Sciences*, *19*(6), Article 1755. <https://doi.org/10.3390/ijms19061755>
- Marelli, B., Ghezzi, C. E., Barralet, J. E., Boccaccini, A. R., & Nazhat, S. N. (2010). Three-Dimensional Mineralization of Dense Nanofibrillar Collagen–Bioglass Hybrid Scaffolds. *Biomacromolecules*, *11*(6), 1470-1479.
<https://doi.org/10.1021/bm1001087>
- Matsiko, A., Levingstone, T. J., O'Brien, F. J., & Gleeson, J. P. (2012). Addition of hyaluronic acid improves cellular infiltration and promotes early-stage chondrogenesis in a collagen-based scaffold for cartilage tissue engineering. *J Mech Behav Biomed Mater*, *11*, 41-52.
<https://doi.org/10.1016/j.jmbbm.2011.11.012>
- Mescher, A. L. (2013). *Junqueira's basic histology: text and atlas* (Vol. 12). McGraw-Hill Medical 13th ed. New York.
- Miosge, N., Hartmann, M., Maelicke, C., & Herken, R. (2004). Expression of collagen type I and type II in consecutive stages of human osteoarthritis [Article]. *Histochemistry and Cell Biology*, *122*(3), 229-236.
<https://doi.org/10.1007/s00418-004-0697-6>

- Miyata, T., Taira, T., & Noishiki, Y. (1992). Collagen engineering for biomaterial use. *Clinical Materials*, 9(3), 139-148. [https://doi.org/https://doi.org/10.1016/0267-6605\(92\)90093-9](https://doi.org/https://doi.org/10.1016/0267-6605(92)90093-9)
- Muthukumar, T., Sreekumar, G., Sastry, T. P., & Chamundeeswari, M. (2018). Collagen as a potential biomaterial in biomedical applications [Article]. *Reviews on Advanced Materials Science*, 53(1), 29-39. <https://doi.org/10.1515/rams-2018-0002>
- Nagai, T., Tanoue, Y., Kai, N., & Suzuki, N. (2015). Characterization of collagen from emu (*Dromaius novaehollandiae*) skins. *Journal of food science and technology*, 52(4), 2344-2351. <https://doi.org/10.1007/s13197-014-1266-1>
- Noorzai, S., Verbeek, C. J. R., Lay, M. C., & Swan, J. (2020). Collagen Extraction from Various Waste Bovine Hide Sources [Article]. *Waste and Biomass Valorization*, 11(11), 5687-5698. <https://doi.org/10.1007/s12649-019-00843-2>
- Olszta, M. J., Cheng, X., Jee, S. S., Kumar, R., Kim, Y.-Y., Kaufman, M. J., Douglas, E. P., & Gower, L. B. (2007). Bone structure and formation: A new perspective. *Materials Science and Engineering: R: Reports*, 58(3), 77-116. <https://doi.org/https://doi.org/10.1016/j.mser.2007.05.001>
- Palmer, L. C., Newcomb, C. J., Kaltz, S. R., Spoerke, E. D., & Stupp, S. I. (2008). Biomimetic systems for hydroxyapatite mineralization inspired by bone and enamel. *Chem Rev*, 108(11), 4754-4783. <https://doi.org/10.1021/cr8004422>
- Parenteau-Bareil, R., Gauvin, R., & Berthod, F. (2010). Collagen-based biomaterials for tissue engineering applications [Article]. *Materials*, 3(3), 1863-1887. <https://doi.org/10.3390/ma3031863>
- Parisi, C., Salvatore, L., Veschini, L., Serra, M. P., Hobbs, C., Madaghiele, M., Sannino, A., & Di Silvio, L. (2020). Biomimetic gradient scaffold of collagen–hydroxyapatite for osteochondral regeneration. *Journal of Tissue Engineering*, 11, 2041731419896068. <https://doi.org/10.1177/2041731419896068>
- Parry, D. A. (1988). The molecular and fibrillar structure of collagen and its relationship to the mechanical properties of connective tissue. *Biophys Chem*, 29(1-2), 195-209. [https://doi.org/10.1016/0301-4622\(88\)87039-x](https://doi.org/10.1016/0301-4622(88)87039-x)
- Pereira, D. R., Reis, R. L., & Oliveira, J. M. (2018). Layered Scaffolds for Osteochondral Tissue Engineering. *Adv Exp Med Biol*, 1058, 193-218. https://doi.org/10.1007/978-3-319-76711-6_9
- Piper, D. W., & Fenton, B. H. (1965). pH stability and activity curves of pepsin with special reference to their clinical importance. *Gut*, 6(5), 506-508. <https://doi.org/10.1136/gut.6.5.506>
- Poole, A. R., Kojima, T., Yasuda, T., Mwale, F., Kobayashi, M., & Lavery, S. (2001). Composition and structure of articular cartilage: a template for tissue repair. *Clin Orthop Relat Res*(391 Suppl), S26-33. <https://doi.org/10.1097/00003086-200110001-00004>
- Rahimi, K., Alizadeh, M., & Abdekhodaie, M. J. (2020, 26-27 Nov. 2020). Comparative study of physical properties of enzymatic in situ hydrogels based on bovine Achilles tendon collagen and rat tail collagen. 2020 27th National and 5th International Iranian Conference on Biomedical Engineering (ICBME),

- Ramesh, S., Tan, C. Y., Aw, K. L., Yeo, W. H., Hamdi, M., Sopyan, I., & Teng, W. D. (2008). Sintering behaviour of hydroxyapatite bioceramics. *Med J Malaysia, 63 Suppl A*, 89-90.
- Ran, X. G., & Wang, L. Y. (2014). Use of ultrasonic and pepsin treatment in tandem for collagen extraction from meat industry by-products. *J Sci Food Agric, 94*(3), 585-590. <https://doi.org/10.1002/jsfa.6299>
- Rezvani Ghomi, E., Nourbakhsh, N., Akbari Kenari, M., Zare, M., & Ramakrishna, S. (2021). Collagen-based biomaterials for biomedical applications [Review]. *Journal of Biomedical Materials Research - Part B Applied Biomaterials, 109*(12), 1986-1999. <https://doi.org/10.1002/jbm.b.34881>
- Sarrigiannidis, S. O., Rey, J. M., Dobre, O., González-García, C., Dalby, M. J., & Salmeron-Sanchez, M. (2021). A tough act to follow: collagen hydrogel modifications to improve mechanical and growth factor loading capabilities. *Materials today. Bio, 10*, 100098. <https://doi.org/10.1016/j.mtbio.2021.100098>
- Schmidt, M. M., Prestes Dornelles, R., Mello, R., Kubota, E. H., Mazutti, M., Kempka, A., & Demiate, I. (2016). Collagen extraction process. *23*, 913-922.
- Seo, S. J., Mahapatra, C., Singh, R. K., Knowles, J. C., & Kim, H. W. (2014). Strategies for osteochondral repair: Focus on scaffolds [Review]. *Journal of Tissue Engineering, 5*. <https://doi.org/10.1177/2041731414541850>
- Sophia Fox, A. J., Bedi, A., & Rodeo, S. A. (2009). The basic science of articular cartilage: Structure, composition, and function [Article]. *Sports Health, 1*(6), 461-468. <https://doi.org/10.1177/1941738109350438>
- Sorushanova, A., Skoufos, I., Tzora, A., Mullen, A. M., & Zeugolis, D. I. (2021). The influence of animal species, gender and tissue on the structural, biophysical, biochemical and biological properties of collagen sponges. *Journal of Materials Science: Materials in Medicine, 32*(1), 12. <https://doi.org/10.1007/s10856-020-06485-4>
- Tamaddon, M., Blunn, G., Tan, R., Yang, P., Sun, X., Chen, S.-M., Luo, J., Liu, Z., Wang, L., Li, D., Donate, R., Monzón, M., & Liu, C. (2022). In vivo evaluation of additively manufactured multi-layered scaffold for the repair of large osteochondral defects. *Bio-Design and Manufacturing, 5*(3), 481-496. <https://doi.org/10.1007/s42242-021-00177-w>
- Tang, S., Vickers, S. M., Hsu, H. P., & Spector, M. (2007). Fabrication and characterization of porous hyaluronic acid-collagen composite scaffolds. *J Biomed Mater Res A, 82*(2), 323-335. <https://doi.org/10.1002/jbm.a.30974>
- Temenoff, J. S., & Mikos, A. G. (2000). Review: tissue engineering for regeneration of articular cartilage. *Biomaterials, 21*(5), 431-440. [https://doi.org/10.1016/s0142-9612\(99\)00213-6](https://doi.org/10.1016/s0142-9612(99)00213-6)
- Thomopoulos, S., Williams, G. R., Gimbel, J. A., Favata, M., & Soslowsky, L. J. (2003). Variation of biomechanical, structural, and compositional properties along the tendon to bone insertion site. *J Orthop Res, 21*(3), 413-419. [https://doi.org/10.1016/s0736-0266\(03\)00057-3](https://doi.org/10.1016/s0736-0266(03)00057-3)
- Thuanthong, M., De Gobba, C., Sirinupong, N., Youravong, W., & Otte, J. (2017). Purification and characterization of angiotensin-converting enzyme-inhibitory

- peptides from Nile tilapia (*Oreochromis niloticus*) skin gelatine produced by an enzymatic membrane reactor. *Journal of Functional Foods*, 36, 243-254. <https://doi.org/https://doi.org/10.1016/j.jff.2017.07.011>
- Wei, W., & Dai, H. (2021). Articular cartilage and osteochondral tissue engineering techniques: Recent advances and challenges. *Bioact Mater*, 6(12), 4830-4855. <https://doi.org/10.1016/j.bioactmat.2021.05.011>
- Wirth, C. J., & Rudert, M. (1996). Techniques of cartilage growth enhancement: a review of the literature. *Arthroscopy*, 12(3), 300-308. [https://doi.org/10.1016/s0749-8063\(96\)90062-6](https://doi.org/10.1016/s0749-8063(96)90062-6)
- Xia, Z., Villa, M. M., & Wei, M. (2014). A biomimetic collagen–apatite scaffold with a multi-level lamellar structure for bone tissue engineering [10.1039/C3TB21595D]. *Journal of Materials Chemistry B*, 2(14), 1998-2007. <https://doi.org/10.1039/C3TB21595D>
- Xia, Z., Yu, X., Jiang, X., Brody, H. D., Rowe, D. W., & Wei, M. (2013). Fabrication and characterization of biomimetic collagen-apatite scaffolds with tunable structures for bone tissue engineering. *Acta Biomater*, 9(7), 7308-7319. <https://doi.org/10.1016/j.actbio.2013.03.038>
- Xu, Q., Torres, J. E., Hakim, M., Babiak, P. M., Pal, P., Battistoni, C. M., Nguyen, M., Panitch, A., Solorio, L., & Liu, J. C. (2021). Collagen- and hyaluronic acid-based hydrogels and their biomedical applications. *Mater Sci Eng R Rep*, 146. <https://doi.org/10.1016/j.mser.2021.100641>
- Xu, S., Gu, M., Wu, K., & Li, G. (2019). Unraveling the Role of Hydroxyproline in Maintaining the Thermal Stability of the Collagen Triple Helix Structure Using Simulation. *The Journal of Physical Chemistry B*, 123(36), 7754-7763. <https://doi.org/10.1021/acs.jpcc.9b05006>
- Yu, L., Cavelier, S., Hannon, B., & Wei, M. (2023). Recent development in multizonal scaffolds for osteochondral regeneration. *Bioact Mater*, 25, 122-159. <https://doi.org/10.1016/j.bioactmat.2023.01.012>
- Yu, L., Rowe, D. W., Perera, I. P., Zhang, J., Suib, S. L., Xin, X., & Wei, M. (2020). Intrafibrillar Mineralized Collagen–Hydroxyapatite-Based Scaffolds for Bone Regeneration. *ACS Applied Materials & Interfaces*, 12(16), 18235-18249. <https://doi.org/10.1021/acsami.0c00275>
- Zeugolis, D. I., Paul, R. G., & Attenburrow, G. (2008). Factors influencing the properties of reconstituted collagen fibers prior to self-assembly: Animal species and collagen extraction method [Article]. *Journal of Biomedical Materials Research - Part A*, 86(4), 892-904. <https://doi.org/10.1002/jbm.a.31694>
- Zhang, H., & Cooper, A. (2007). Aligned Porous Structures by Directional Freezing. *Advanced Materials*, 19, 1529-1533. <https://doi.org/10.1002/adma.200700154>
- Zhou, H., Chen, R., Wang, J., Lu, J., Yu, T., Wu, X., Xu, S., Li, Z., Jie, C., Cao, R., Yang, Y., Li, Y., & Meng, D. (2020). Biphasic fish collagen scaffold for osteochondral regeneration. *Materials & Design*, 195, 108947. <https://doi.org/https://doi.org/10.1016/j.matdes.2020.108947>



OHIO
UNIVERSITY

Thesis and Dissertation Services